TRIUMF

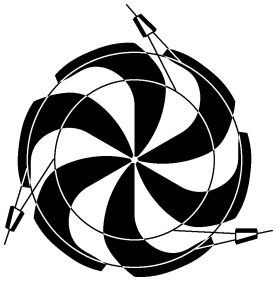

ANNUAL REPORT
SCIENTIFIC ACTIVITIES
1998

CANADA'S NATIONAL MESON FACILITY
OPERATED AS A JOINT VENTURE BY:

MEMBERS:

UNIVERSITY OF ALBERTA
SIMON FRASER UNIVERSITY
UNIVERSITY OF VICTORIA
UNIVERSITY OF BRITISH COLUMBIA

ASSOCIATE MEMBERS:

UNIVERSITY OF MANITOBA
UNIVERSITÉ DE MONTRÉAL
UNIVERSITY OF TORONTO
UNIVERSITY OF REGINA
CARLETON UNIVERSITY
QUEEN'S UNIVERSITY

UNDER A CONTRIBUTION FROM THE
NATIONAL RESEARCH COUNCIL OF CANADA

APRIL 1999

The contributions on individual experiments in this report are outlines intended to demonstrate the extent of scientific activity at TRIUMF during the past year. The outlines are not publications and often contain preliminary results not intended, or not yet ready, for publication. Material from these reports should not be reproduced or quoted without permission from the authors.

Experiment 684
μSR spin relaxation studies of small molecules in the gas phase
(J. Pan, D. Fleming, UBC–TRIUMF)

This experiment studies the muon spin relaxation in some simple gas-phase systems with the primary goal of measuring the chemical reaction rates. This year, the focus of our research is on the low temperature studies of the Mu + CO and Mu + NO reactions with two different moderators, He and N_2, in both longitudinal (LF) and transverse (TF) magnetic fields.

A total of five weeks of experiments were carried out on M9 at pressures from 60 to 500 bar and temperatures from 140 K to 300 K.

Mu + NO+ N_2

For the reaction of Mu + NO +N_2, the moderator dependence is apparently different from that observed at room temperature where the bimolecular reaction rate constant is linearly proportional to total moderator concentration.

At 227 K, the Mu + NO reaction rate constants were measured in LF. The results are shown in Fig. 60. The quadratic moderator dependence indicates that the dominant reaction mechanism is different than at room temperature. The spin exchange rate constant, which is moderator independent at room temperature, also strongly depends on the total pressure. The NO dimer formation could not account for the experimental results. One explanation is that the intermediate-complex forming mechanism, which is probably negligible at room temperature, becomes more important at lower temperatures because there are more Learnard Jones molecular complexes ($NO{\cdot}N_2$) formed. More likely, both energy transfer mechanism and the intermediate complex mechanism contribute to the total reaction. Unfortunately, these two contributions cannot be separated under the current experimental conditions. More temperature variation studies are required to confirm the reaction mechanisms involved.

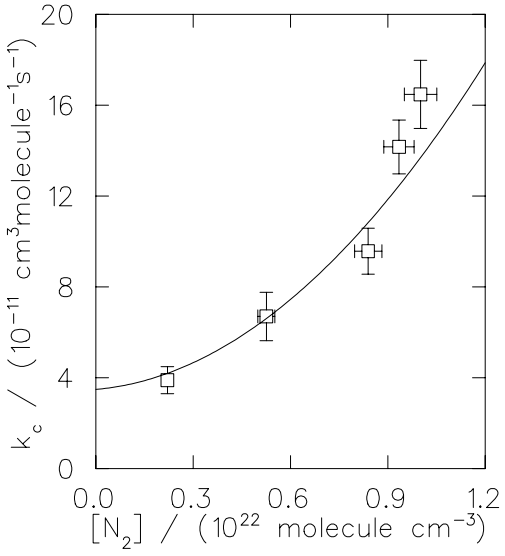

Fig. 60. Mu + NO at 227 K.

Mu + CO

The Mu + CO reactions were studied with both He and N_2 moderator in TF (5 and 60 G). At all temperatures, the moderator dependence of the chemical reaction rate constants are quadratic in N_2. Figure 61 shows a typical plot of the total reaction rates which include both chemical and spin relaxation contributions.

In He, however, since the concentration range is relatively small, there is no obvious deviation from a linear dependence at pressures higher than 200 bar (Fig. 62). Experiments extending the pressure range down to a few bar are planned for the coming beam period.

Again, the intermediate-complex and energy transfer reaction channels and the coupling of both channels are expected. The results certainly ruled out a straightforward energy transfer mechanism even at room temperature. Currently, the reaction mechanism is not completely understood. Further measurements at lower pressures (0–60 bar) are under way. Theoretical investigation of the reaction mechanisms is also being actively pursued.

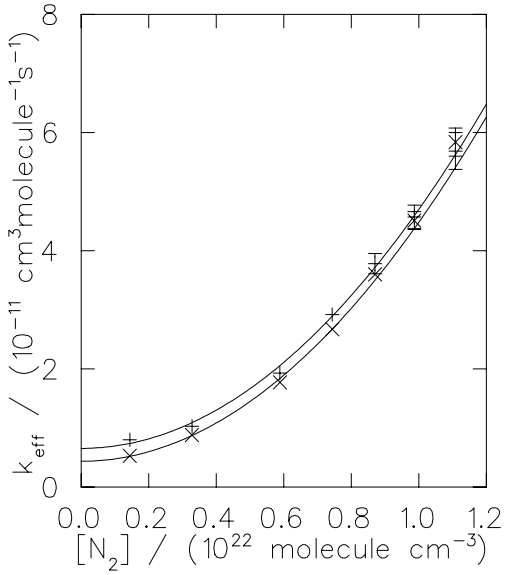

Fig. 61. Mu + CO + N_2 at 180 K. Lower curve: 5 G TF. Upper curve: 60 G.

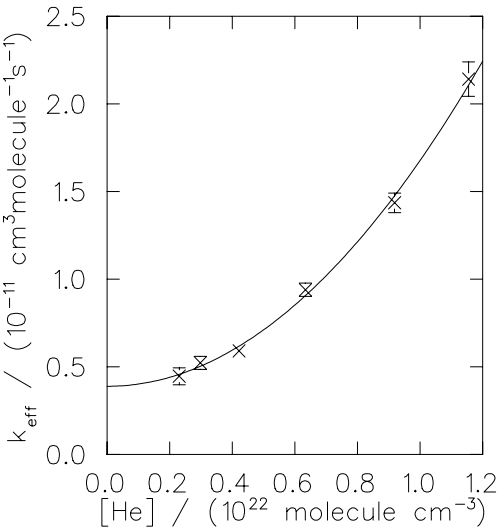

Fig. 62. Mu + CO + He at 178 K. Measurements were made only at 5 G TF.

Experiment 691
The vortex cores in type-II superconductors
(J.H. Brewer, CIAR/UBC; J.E. Sonier, CIAR/Los Alamos)

In 1998 we continued our investigation of the vortex core size r_0 in type-II superconductors. Previous studies under Expt. 691 found a novel increase in r_0 at low magnetic fields in the conventional superconductor $NbSe_2$ [Phys. Rev. Lett. **79**, 1742 (1997)] and in the oxygen deficient high-T_c superconductor $YBa_2Cu_3O_{6.60}$ [Phys. Rev. Lett. **79**, 2875 (1997)]. The temperature dependence of r_0 in both of these compounds was also found to deviate from the known theoretical predictions at that time.

Much of what is known about high-T_c superconductors comes from experiments on compounds which are doped to give the maximum value of T_c. Thus, it was of great interest to check the size, temperature and magnetic field dependence of r_0 in optimally doped $YBa_2Cu_3O_{6.95}$, with a maximum T_c of 93 K. Furthermore, since the considerable progress in our μSR measurements in the high-T_c materials in recent years is due in part to the improvements in crystal growth, it was imperative that we verified the influence of extrinsic sample effects on our findings.

Our main findings from high-statistic TF-μ^+SR measurements on several twinned and detwinned crystals of $YBa_2Cu_3O_{6.95}$ are summarized in Fig. 63. The temperature dependence of r_0 is observed to be weak at low T (compared to $NbSe_2$) and r_0 is found to increase at lower magnetic fields, where it approaches an extraordinarily large value of about 100 Å. Furthermore, we find that the absolute value of r_0 is essentially the same in all samples studied.

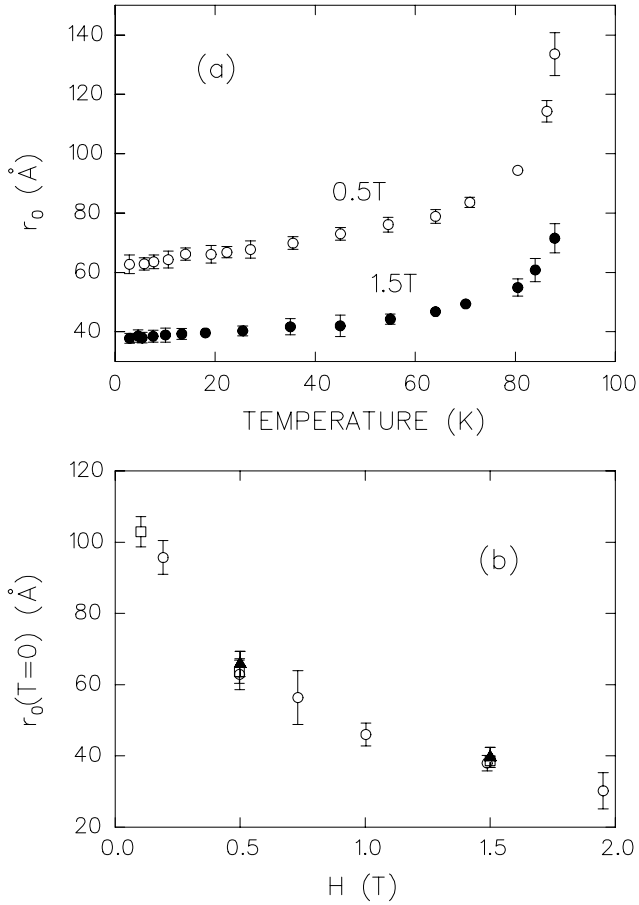

Fig. 63. (a) The temperature dependence of r_0 at $H =$ 0.5 T (open circles) and 1.5 T (solid circles) in twinned $YBa_2Cu_3O_{6.95}$. (b) The magnetic field dependence of r_0 extrapolated to $T = 0$ in twinned (both open circles and squares) and detwinned (solid triangles) crystals of $YBa_2Cu_3O_{6.95}$.

In the wake of these and our previous measurements under Expt. 691, numerous theoretical studies are now aimed at redeveloping the general picture of the vortex state. In particular, considerable effort is being made to understand why the vortex cores expand at low magnetic fields. We surmise from our μSR experiments that this is a general property of all superconductors in the vortex state. Recently, the expansion of the vortex core size in $NbSe_2$ was used to explain the low magnetic field anomaly of the electronic specific heat observed in conventional s-wave superconductors [Sonier *et al.* (submitted to Phys. Rev. Lett.)]. Our measurements of r_0 are now being seriously considered in the interpretation of other experiments performed in the vortex state.

In 1998 we also carried out both TF and LF μSR measurements in the underdoped superconductor $YBa_2Cu_3O_{6.57}$ in an effort to find evidence for the existence of antiferromagnetic (AFM) vortex cores, as predicted in the proposed $SO(5)$ theory of high-T_c su-

perconductivity [Zhang, Science **275**, 1089 (1997)]. A similar experiment performed under Expt. 691 in 1997 suffered from distortions in the LF time spectra and a lack of statistics in the TF lineshapes. Despite improvements in both of these areas as well as an improvement in sample quality, no definitive conclusion could be made in the 1998 version of this experiment. Instead we determined that if there are indeed AFM moments in the vortex cores, they are fluctuating at a rate too fast or too slow to be unambiguously observed with the current sensitivity of LF-μSR measurements. Similarly, evidence for their existence from TF-μSR lineshapes continues to suffer from the difficulties associated with transforming the spectra into the frequency domain. Both advancements in μSR data collection and analysis techniques are needed to further this investigation.

Present status of Expt. 691

In December the decision was made to replace Expt. 691 with several new experiments (i.e. Expts. 846, 847 and 848) to carry out a thorough and detailed investigation of important but specific topics of the vortex state in high-T_c superconductors, which are uniquely suited for μSR.

Experiment 713
Muonium chemistry in supercritical water
(P.W. Percival, SFU)

The properties of water change markedly when it is subjected to temperatures and pressures near or above the critical point (374°C, 220 atm). The ionic product falls by many orders of magnitude and the dielectric constant is reduced to values typical of organic solvents. It is even possible to sustain a flame in supercritical water, by injecting oxygen into an aqueous solution of methane. This has led to several investigations of the potential of supercritical water (SCW) oxidation as a means for hazardous waste destruction, including chemical weapons and the clean-up of nuclear processing sites.

A significant hurdle to practical development of SCW destruction facilities is the current lack of detailed knowledge of physical, chemical and transport properties of supercritical fluids at the molecular level, particularly free radical chemistry and kinetics under such conditions. Probing reactions at the molecular level clearly calls for spectroscopic methods. However, there are considerable experimental difficulties, and until recently most studies were limited to stable species in solution. In any event, optical spectroscopic methods are not suited to the study of transient free radicals. The preferred option for free radical characterization is ESR, but the severe practical problems involved have precluded the necessary development.

TRIUMF Expt. 713 was designed to explore the potential of μSR to probe SCW chemistry, using muonium as a model for the hydrogen atom. The first stage of the project involved development of a sample cell with a window which allows penetration of muons (typically 70 MeV/c momentum), yet is strong enough to withstand pressures up to 500 atm and temperatures to 500°C. The apparatus has been used for μSR experiments on water over a wide range of temperatures and pressures, up to 350 atm and 420°C, corresponding to water densities from below 0.1 g cm^{-3} to 1.0 g cm^{-3}. We have demonstrated that muonium is long-lived over the whole range of conditions and that the muonium signal amplitude and hyperfine constant vary with density. Our first measurements of muonium kinetics in sub- and super-critical water revealed remarkable effects – the rate constant for a spin exchange reaction was found to rise with temperature at a rate much less than that predicted by simple diffusion theory, and then to go through a maximum. We suspect this signals differential location of ions and hydrophobic solutes (in this case Mu) in water clusters and voids, respectively. If so, this has important practical consequences for the performance of a SCWO reactor.

In the summer we achieved the final goal of Expt. 713 – successful detection of muonium-substituted free radicals in supercritical water. We were able to obtain transverse field μSR spectra of cyclohexadienyl and tert-butyl in aqueous solutions of their precursors, benzene and isobutene, respectively. Examples are given in Figs. 64 and 65.

We believe this is the first direct identification of organic free radicals in sub- and super-critical water by *any* technique. It opens up a wide area of free radical chemistry to detailed study. Free radicals almost

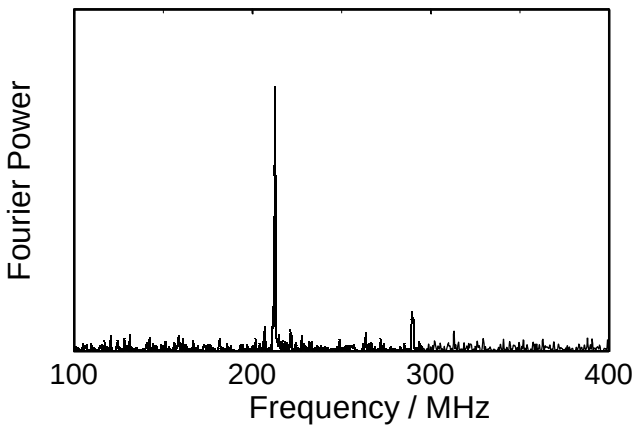

Fig. 64. Fourier power μSR spectrum from a solution of benzene in water at 230°C, 250 atm, in a transverse field of 2.05 kG. The peaks at 210 and 290 MHz are due to the cyclohexadienyl radical C_6H_6Mu. A large diamagnetic signal is off scale.

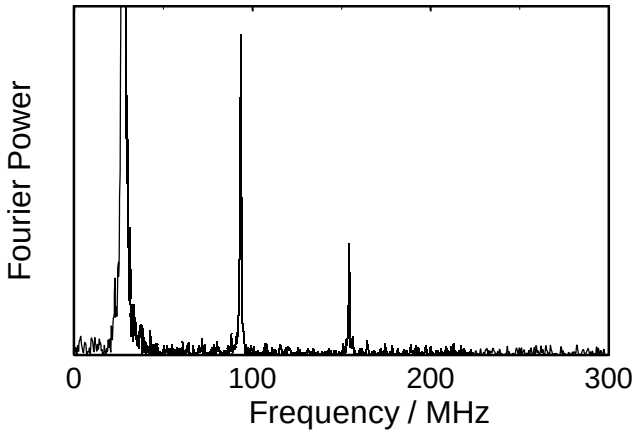

Fig. 65. Fourier power μSR spectrum from a solution of tert-butanol in water at 385°C, 250 atm, in a transverse field of 2.05 kG. The truncated peak at 28 MHz is due to muons in a diamagnetic environment. The other two peaks arise from the tert-butyl radical $MuCH_2C(CH_3)_2$.

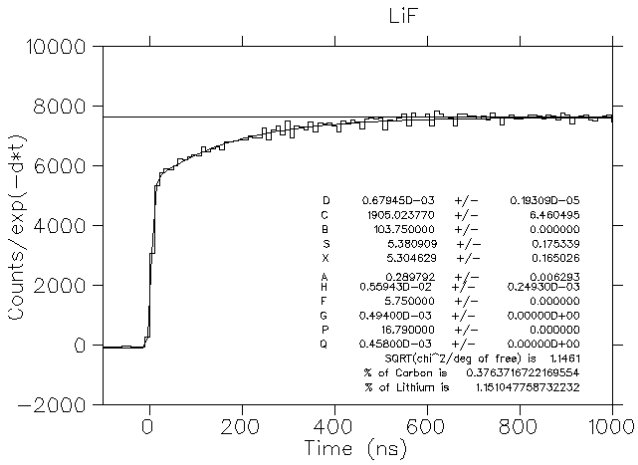

Fig. 66. Time spectrum of neutrons after muon capture on LiF with the muon lifetime in LiF divided out.

certainly play a major role in SCW waste destruction, but studies are typically limited to end-product analysis. Furthermore, 'aquathermolysis', the reactions of organic molecules in superheated water, is a growing area of organic chemistry, and the ability to detect radical intermediates will surely aid its development.

Although we detected radicals in SCW this was by transverse field (1–2 kG) μSR, using samples of almost molar concentration. Full characterization (measurement of proton hyperfine coupling constants as well as that of the muon) and detection at low concentrations requires muon level-crossing spectroscopy (μLCR).

The necessary spectrometer (HELIOS) exists but the sample access and detector geometry is completely different, since HELIOS is a superconducting solenoid while SFUMU, the μSR spectrometer used for Expt. 713 is based on an open Helmholtz pair. Thus, the SCW sample cell must be completely re-engineered. All the inlets/outlets to the cell must be fitted at the rear, and the cell must be better insulated (probably water cooled) to protect a new set of custom built plastic scintillators. This project will be pursued under a new TRIUMF experiment, Expt. 842, which was approved at the December meeting of the EEC.

Experiment 717
Muonic hyperfine transition rates in light nuclei
(T.J. Stocki, D.F. Measday, UBC)

The muonic hyperfine transition rates were measured in LiF, $(CF_2)_n$, Na, NaH, Al, $LiAlH_4$ and for the first time in K and P. These measurements were performed by detecting neutrons via liquid scintillators. The most precise measurement of the muonic hyperfine transition rate was made on LiF. Figure 66 shows the data and the fit for the neutron time spectrum for LIF. No chemical effect was observed when comparing the transition rates in LiF and $(CF_2)_n$, Na and NaH, Al and $LiAlH_4$. In the case of P and K the newly measured hyperfine transition rates are $48 \pm 5\ \mu s^{-1}$ (this value is model dependent) and $25 \pm 15\ \mu s^{-1}$.

Nitrogen should not have a hyperfine transition if the only hyperfine transition process is through Auger emission, because the hyperfine splitting energy is smaller than the energy needed for the Auger process. So confirmation of a previous nonzero measurement of a hyperfine effect in ^{14}N was attempted. This search for a hyperfine effect in ^{14}N was performed by detecting neutrons and γ-rays in two separate experiments. In the neutron experiment liquid scintillators were used to measure the time spectra of the electrons and neutrons. It was found that the muon lifetime obtained from the neutron time spectrum was different than the lifetime measured in the electron time spectrum. This difference may indicate a hyperfine transition in nitrogen. In the case of the γ-ray experiment, which was performed using two high purity germanium detectors, the results lacked sufficient statistics.

During this nitrogen γ-ray experiment, much new information was obtained. The yields of γ-ray produced from muon capture in ^{14}N were measured. Previously only the yield from one γ-ray had been measured. In this experiment yields from three γ-rays in ^{14}C, from three γ-rays in ^{13}C, from one γ-ray in ^{12}C, and two γ-rays in ^{10}B were measured. From these yields, the nuclear level yields were obtained. In addition, the energies of two γ-rays in ^{14}C were measured more accurately than before; these γ-rays are at energies of 7016.8 ±1.3 keV (shown in Fig. 67) and 6730.6 ± 1.0 keV.

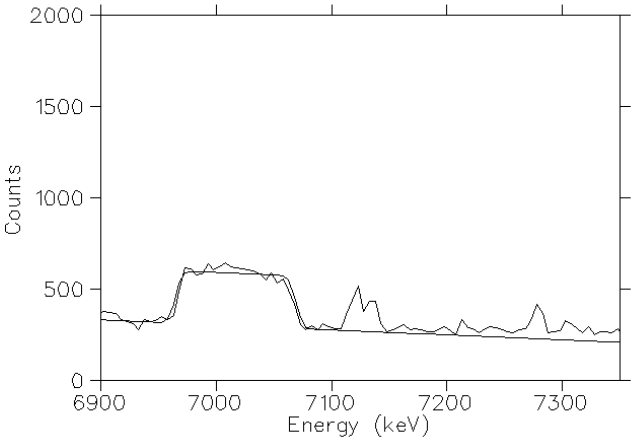

Fig. 67. The 7017 keV γ-ray and its doppler broadend fit.

Experiment 720/750
Muonium as a light isotope of hydrogen
(D.C. Walker, UBC)

Our major publication during the year was an Invited Faraday Research article [J. Chem. Soc., Faraday Trans., **94**, 1 (1998)] (including one of the figures on the journal cover). This provides an overview of our work on muonium atoms (Mu) in water. It shows the variation of reactivity of Mu with different types of additives to the water. Mu is shown to react according to classical reaction-dynamic principles in one type, and according to quantum-mechanical principles in the other.

The hundred or so solutes discussed fall into two camps: (i) those whose reactivity towards Mu – compared to ordinary H atoms – gives a kinetic isotope effect (KIE) which can be explained, to a good approximation, by classical transition state theory (corresponding to enhanced reaction path barriers of H over Mu, but higher encounter frequencies of Mu over H), Table X; and (ii), those reactions which give contrary KIEs and which can only be explained by the dominance of quantum effects. In the latter category lie reactions in which Mu adds to an aromatic ring at the ortho-meta-para positions in the opposite sense found for H atom addition; and Mu reactions in which Mu adds to the O atom of a carbonyl group in a ketone (where H adds to the C atom), as demonstrated in Table XI.

There is another overall feature revealed in this review: Mu's reactions as a reducing agent fall directly between those of H atoms and hydrated electrons ($e^-_{(aq)}$). This in-between character is expressed in the relative reaction rates of Mu compared to H and $e^-_{(aq)}$, as in Table XII.

Table X. A sample of observed k_M values and KIEs (k_M/k_H) in water at ∼295 K for reactions which seem to involve the same mechanism and form isotopomeric products with Mu and H.

Solute (type of Mu reaction)	$k_M/M^{-1}s^{-1}$	KIE	Origin of KIE
$H_2C_2O_4/HC_2O_4^-$, pH=1 (addition)	3.4×10^8	850	tunneling
$C_2O_4^{2-}$, pH=8 (addition)	5.4×10^6	>300	tunneling
OH^- (acid, Mu^+ transfer)	1.7×10^7	0.7	none
uracil (addition to C(5) & C(6))	6×10^9	16	addition
thymine (addition to C(5) & C(6))	3×10^9	5	steric hindrance
benzene (addition to ring)	3×10^9	3	solvation
styrene (addition to side chain)	2×10^{10}	3	diffusion-limited
acrylic acid (addition to vinyl)	1.6×10^{10}	4.5	diffusion-limited
O_2 (spin-exchange + combination)	2.4×10^{10}	1.5	diffusion-limited
Ag^+ (reduction to Ag^o)	1.6×10^{10}	0.8	diffusion-limited
2-propanol (abstraction)	$1.0(\pm0.3)\times10^6$	0.015	ZPE effect

Table XI. A sample of k_M values and observed KIEs in water at ∼295 K for representative solutes which react differently towards Mu and H.

Solute	k_M	$KIE_{(obs)}$	Mu reaction	H reaction
acetone	1.0×10^8	75	addition to O	abstraction of H ($\frac{2}{3}$)
butanone	1.0×10^8	4.5	addition to O	abstraction of H (≥90%)
CH_3CSNH_2	3×10^{10}	5	addition to C	addition to S?
pyridine	5.8×10^9	10	addition to C	addition to N?
pyrazine	7.7×10^9	26	addition to C	addition to N?
benzoic acid	7.5×10^9	8	addition to C	addition to C
Cr^{3+} ions	$2–6\times10^{10}$	$>10^4$	spin exchange	reduction to Cr^{2+}

Table XII. Examples of different reaction types which illustrate that Mu lies between H and e^-_{aq} in its reactivity. These rate constants refer to aqueous solutions at ∼295 K: k_e for e^-_{aq}, k_M for Mu, and k_H for H, all in units of 10^7 $M^{-1}s^{-1}$.

Solute	k_e	k_M	k_H
chloroacetic acid	69	0.23	0.013
N_2O	900	6.5	0.21
2-propanol	<0.01	0.1	7.4
nitrate ions	970	150	0.14
oxalate ions (pH=8)	3.1	0.54	<0.004
acetone	650	10	0.1
Tl^+	2000	80	4.1
cytosine (DNA)	1300	300	9.2

Experiment 724
Effects of dilute (Cu,Zn) substitution in spin gap system $SrCu_2O_3$
(M.I. Larkin, G.M. Luke, Y.J. Uemura, Columbia; M. Takano, Kyoto)

Spin systems having spin gaps and a singlet ground state are of great interest due to the quantum nature of the ground state, and superconductivity obtained by charge doping in some systems. Spin-ladder systems have spins arranged in a ladder geometry. In copper-oxide spin ladder compounds, nearest neighbour spins on a ladder and a rung, in this case spin-1/2 Cu^{2+}, are anti-ferromagnetically coupled via 180° Cu-O-Cu bonds with J on the order of 1,000–2,000 K. Inter-ladder coupling occurs via 90° Cu-O-Cu bonds and is geometrically frustrated, strongly reducing the effective coupling, and making the system quasi-1 dimensional. The two-leg ladder system $SrCu_2O_3$ has been seen in susceptibility and neutron experiments to have a spin-gapped singlet ground state with the gap energy $\Delta \approx$680 K. Our previous μSR experiments at TRIUMF confirmed an absence of magnetism down to 20 mK, the lowest measured temperature.

In spite of such a large value for the gap energy of the singlet state which may be naively related to the robustness of the state, a cusp in the magnetic susceptibility suggesting static magnetic freezing has been observed in the Zn-doped 2-leg ladder systems where Cu was substituted with non-magnetic Zn, even at a Zn concentration x of 1% or smaller. We recently performed μSR measurements on ceramic samples of $Sr(Cu_{1-x}Zn_x)_2O_3$ for $0.003 \leq x \leq 0.07$ at beam lines M13 and M15, both in conventional gas-flow cryostats and a dilution refrigerator. In all these Zn-doped 2-leg ladder samples, the relaxation rate of the muon spin exhibits rapid increase with decreasing temperature below T_N in zero external field, with clear decoupling in longitudinal fields, indicating onset of static spin freezing.

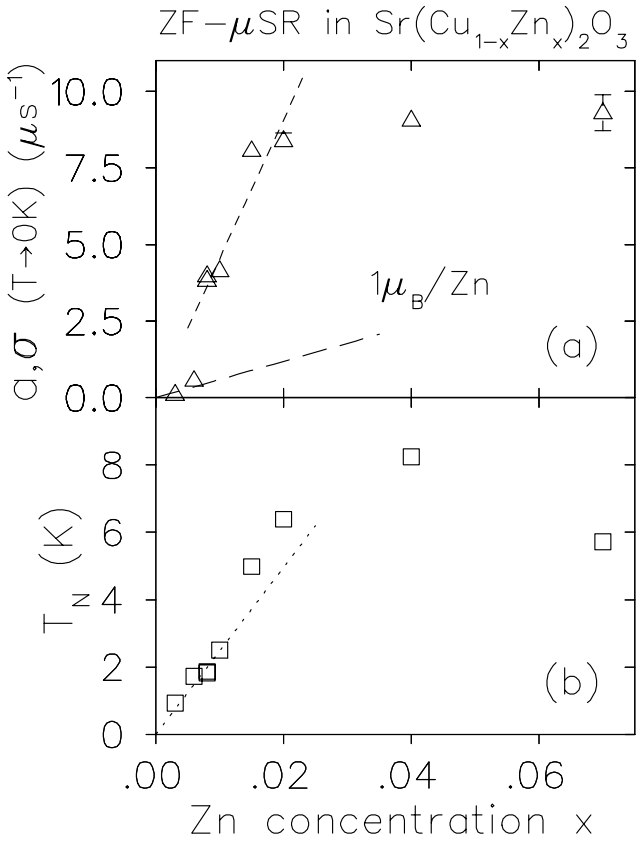

Fig. 68. (a) saturated μSR static relaxation rate (limit as $T \to 0$ K), proportional to the saturated moment size, vs. Zn concentration x. The long-dashed line indicates the relaxation expected for $1\mu_B$ of moment liberated by each substituted Zn. Note the jump from 0.6% to 0.8%. (b) The Néel temperature T_N vs. Zn concentration x. T_N linearly increases with x for low x, as has also been seen in bulk measurements, without a pronounced jump.

In Fig. 68 we show the muon relaxation rate extrapolated to zero temperature (saturated relaxation rate), and T_N vs. Zn concentration x. We see that at low Zn concentration, the relaxation rate is consistent with $1\mu_B$ of moment liberated for each Zn atom. With increasing Zn concentration, the saturated relaxation rate increases quite sharply and non-linearly. There is an abrupt change near 0.8% Zn substitution. At higher concentration, the relaxation rate increases linearly with x until it saturates around 2%. In contrast to the relaxation rate, the Néel temperature T_N determined by μSR does not show any anomaly and increases linearly with increasing x, as was found in other bulk measurements.

The μSR line shapes for $x < 0.008$ are consistent with dilute, random moments, while those for $x > 0.008$ are consistent with spatially denser moments. An absence of clear precession at all x values indicates randomness in the ordered moment size and/or frozen spin orientation.

These results demonstrate that a crossover from

freezing of dilute isolated spins to freezing of the spin network extending presumably to the entire system occurs around $x = 0.008$. A rather high Néel temperature observed even for systems with $x < 0.008$ indicates that singlet spin pairs between unpaired Cu moments play a role in increasing exchange coupling. For $x > 0.008$, the saturated relaxation rate increases linearly with Zn concentration, indicating an increase of the average ordered moment size per Cu. Simulation studies are under way on line shapes and relaxation rates for selected values of spin correlation length and ordered moment size, to consider the present results in terms of characteristic length scale(s) of the 2-leg ladder system.

Experiment 746
Muonium in Si
(B. Hitti, S.R. Kreitzman, TRIUMF)

The structure and dynamics of muonium (Mu=μ^+e^-) in semiconductors have long been recognized as directly relevant to understanding the analogous hydrogen defect centres. To study the dynamics of transitions between the muonium states in Si we employed two muon spin resonance (μSR) spectrometers developed at TRIUMF.

The radio frequency (rf-μSR) spectrometer (10 to 200 MHz) was mainly used to measure the temperature dependence of the diamagnetic amplitude in p-type and n-type Si samples of various dopant concentrations. The rf data show a complicated set of transitions active during the muon lifetime and involving four separate muonium states. Two types of neutral muonium centres are observed in Si at low temperature, the stable configuration has the muon at or near a bond-centre site, Mu^0_{BC}; the second configuration is metastable and is located within the tetrahedral region, Mu^0_T. In addition to the neutral states, charged muonium centres occur. In p-type Si, the charge centre is positive and resides near the BC site, Mu^+_{BC}; while the negative charge state is observed in the moderately to heavily doped n-type samples and is stable at the T site, Mu^-_T. Recent analyses have enabled us to infer parameter values describing the dynamics of muonium in silicon and in particular to determine for the first time ever the binding energy of the negative muonium ion Mu^-_T. This work is complete and has been accepted for publication in Physical Review B [Hitti *et al.* (in press)].

The microwave (μw-μSR) spectrometer (0.8 to 2 GHz) operates at higher frequency than the rf which allows high field measurements to be made for tetrahedral muonium. This avoids low field broadening that is normally present due to various interactions. We used the μw spectrometer to measure the amplitude of the neutral state Mu^0_T at low temperature in Si and

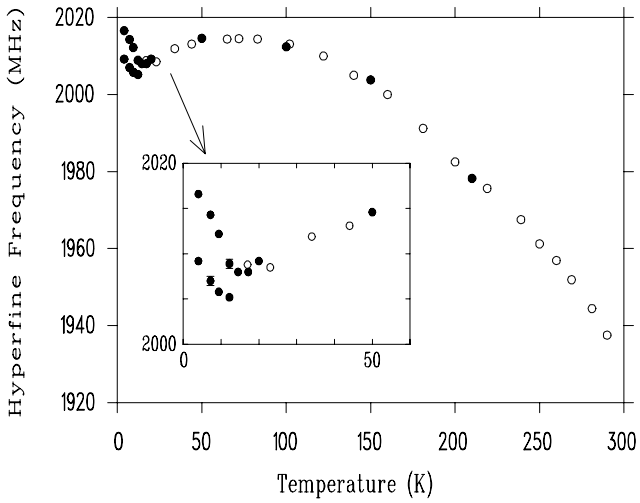

Fig. 69. The Mu^0_T hyperfine frequency in Si as a function of temperature. The open circles are the values measured by Holzschuh [*op. cit.*], the filled circles are from our μw data.

observed unexpected structure. Below 14 K two signals corresponding to two different values of the hyperfine parameter were observed for the first time. This new result appears to be related to the anomaly in the measured hyperfine frequency of Mu^0_T in Si below 50 K first reported by Holzschuh in 1983 [Phys. Rev. **B27**, 102 (1983)]. In Fig. 69 the values of the hyperfine frequency obtained from the μw experiment (filled circles) and those measured by Holzschuh (open circles) are plotted as a function of temperature. Holzschuh used a zero field high timing resolution apparatus and directly measured the transition between the triplet and singlet energy levels of Mu^0_T in Si. The agreement between the two techniques is very good down to 20 K, the lowest temperature measured by Holzschuh.

A satisfactory explanation of this structure and the temperature dependence is lacking. There is indirect evidence of rapid long range tunneling of Mu^0_T in Si which makes two distinct structures with different hyperfine values hard to understand. Experiments using the high magnetic field high timing resolution apparatus are planned and should provide additional information on whether one of the signals is related to delayed formation of Mu^0_T and/or muons stopped close to a ^{29}Si isotope.

Experiment 749
Muonium-substituted free radicals
(P.W. Percival, SFU)

The purpose of Expt. 749 is to study the structure and intramolecular motion of organic free radicals. Muon hyperfine constants are measured by transverse-field muon spin rotation (μSR) and, where necessary, radio frequency muon spin resonance (rf-μSR). Other

hyperfine constants are determined by muon level-crossing resonance (μLCR). Of recent interest are the muonium adducts of fullerenes and various polyaromatic hydrocarbons which can be viewed as fragments of fullerenes. The overall question being pursued is: How does curvature of an unsaturated carbon skeleton affect radical adduct formation?

In the summer we investigated fluoranthene (Fig. 70). The transverse field μSR spectrum (Fig. 71) shows the presence of five radicals – note that there are two almost degenerate signals close to 60 MHz. Each radical gives rise to a pair of muon precession frequencies, but only the low frequencies' signals are visible in the range displayed in Fig. 71. The radicals are formed by Mu addition to different carbon sites in fluoranthene, which has in all 9 unique carbons: *1,2,3,7,8,11,12,15,16*.

To identify the sites of Mu addition we turned to muon level-crossing spectroscopy (μLCR). There is a rich spectrum, as evident from Fig. 72. Each resonance

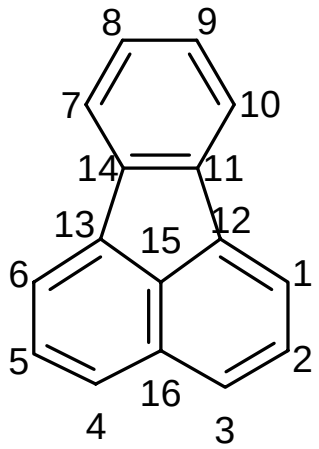

Fig. 70. Fluoranthene, a polyaromatic hydrocarbon. Not shown are the hydrogen atoms attached to carbons *1–10*.

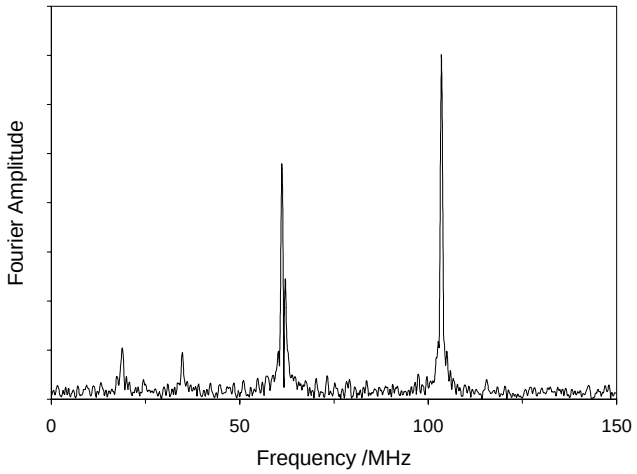

Fig. 71. Part of the Fourier μSR spectrum from pure liquid fluoranthene at 117°C in a transverse field of 17.34 kG.

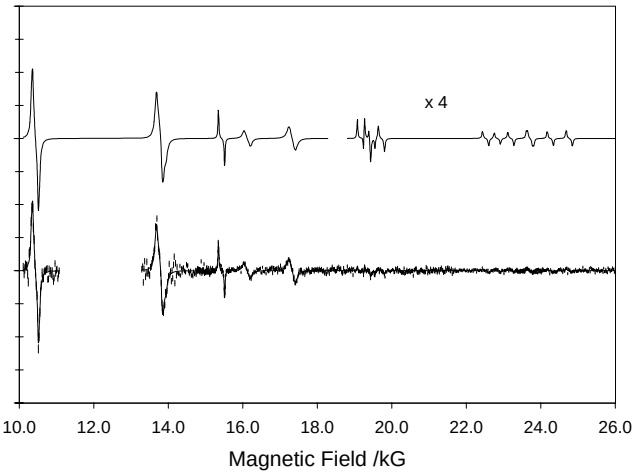

Fig. 72. μLCR spectrum from pure liquid fluoranthene at 117°C. The solid curve represents the best fit to the data points. For clarity it is also redrawn with an offset, and with part magnified to show the weak resonances at high field.

corresponds to a particular value of a proton hyperfine constant (hfc). Some of the resonances are due to -CHMu- groups, i.e. the relevant radical is formed by addition of Mu to a carbon to which a H atom is bound. Such resonances are relatively easily identified, as the H and Mu atoms are effectively isomers, subject to the same electron spin distribution. There is a trivial isotope effect, due to the different magnetic moments of the proton and the muon, but there is also an effect which has been ascribed to zero-point vibrations of the C–Mu bond. This latter effect has been well characterized in other similar radicals (cyclohexadienyl and pyrenyls) and amounts to a factor of about 1.2 in favour of the muon hfc. Thus, the resonances at 10.43, 13.77, 13.86, 16.12 and 17.33 kG are assigned to -CHMu- structures of the five radicals detected by transverse field μSR.

The remaining resonances are all consistent with so-called α Hs – H atoms attached to carbon sites with significant unpaired electron spin density. Their hyperfine constants are predicted to be *negative*, as opposed to the positive hfcs characteristic of the -CHMu- groups. A preliminary assignment of individual resonances with particular muon hfcs (i.e. particular radicals) gives plausible values for the corresponding proton hfcs, and the predicted narrow linewidths are also in accord with experiment. Final confirmation and assignment of the measured hyperfine constants to specific radicals awaits quantum chemical calculation of the various isomeric radical structures and spin distributions. However, it already seems clear that only five radicals are formed, and that these correspond to Mu addition at carbons *1+6, 2+5, 3+4, 7+10, and 8+9*. There is no sign radicals formed by Mu addition at carbons *11–16*.

Experiment 751
μSR measurements of off-axis internal magnetic fields in anisotropic superconductors
(W.J. Kossler, College of William and Mary)

The major accomplishments of this experiment so far have been:

- The discovery of magnetic transparency of the ab planes to magnetic fields in the superconducting state of BSCCO.
- The observation of longitudinal field depolarization associated with vortex motion.

Transparency of the ab planes in highly anisotropic superconductors

For many anisotropic superconductors, e.g., $YBa_2Cu_3O_7$ (YBCO) the anisotropy may be represented by an effective mass tensor. Then one finds the fields from the minimization of the free energy:

$$\mathcal{F} = \frac{1}{8\pi}\int_V (b^2 + \lambda^2 m_{ij}(\nabla \times \vec{b})_i(\nabla \times \vec{b})_j)dV \qquad (1)$$

The effective reduced mass tensor m_{ij} expresses the anisotropy and m_c/m_{ab}, the ratio of the mass along **c** to mass along the **a** or **b** is a measure of this anisotropy. For an isotropic superconductor $m_{ij} = \delta_{ij}$ and the currents form vortices independent of crystalline axis (top of Fig. 73). For YBCO this mass ratio is about 25. The vortices that then form have currents which are not everywhere perpendicular to their axes. This is shown in the lower left portion of Fig. 73. This model produces vortices of a 3D tilted nature and has average fields parallel to the axis of this tilted vortex even for arbitrarily large masses along the **c** axis.

For BSCCO the anisotropy is much larger than for YBCO and is of order 3000. Such extreme anisotropy had previously led Lawrence and Doniach to introduce a model in which the weak inter-planar coupling along the **c** axis occurs via Josephson tunneling. Clem introduced the notion of "pancake" vortices which are confined to the CuO planes for these extremely anisotropic systems. The general picture is shown schematically in the bottom centre of Fig. 73. Clem and Artemenko and Kruglov have shown how one may calculate the magnetic fields of pancake arrays. Clem has further shown that the equilibrium arrangement in the limit of very weak coupling is like that shown in the lower right portion of Fig. 73, i.e., the pancakes of current line up on top of each other along the **c** axis while the field in the **ab** planes penetrates freely and unshielded.

When cosine transforms are performed on P_{yz}(t) and $P_{yy}(t)$, (initial polarization along y and detection along z and y respectively), only those components

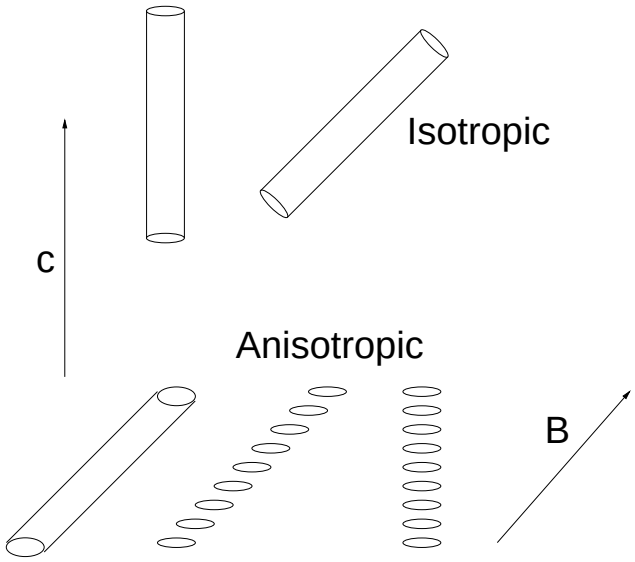

Fig. 73. For the isotropic case a vortex may be considered to be a tube like structure oriented in any direction. This is illustrated in the top portion. For the anisotropic case, one may have tube like structures with currents tipped with respect to the axis or separated pancakes of current, see the text.

with b = ω/γ_μ will be selected from the distribution of fields. We thus obtain the Fourier amplitudes:

$$\tilde{P}_{yz}(\omega) = \frac{dn}{db}\frac{< b_z b_y(\omega) >}{b^2} \qquad (2)$$

and

$$\tilde{P}_{yy}(\omega) = \frac{dn}{db}\frac{< b_x^2(\omega) + b_z^2(\omega) >}{b^2}\,. \qquad (3)$$

Here the terms enclosed within $< \ldots >$ refer to the average value of the expression at the given ω. Note that if the internal fields pointed everywhere in the same direction, as in isotropic superconductors, the ratio of fields factors in these cosine transforms would be dependent on the direction, but not the magnitude of the field. Then $\tilde{P}_{yz}(\omega) \propto \tilde{P}_{yy}(\omega)$ and the cosine transforms have exactly the same shape.

We have applied this technique to a BSCCO sample. A field of approximately 100 G was applied 45 degrees from the beam axis in the **yz** plane, (y vertical, and z along the beam). The sample was field cooled to 2 K. The cosine transforms of data taken in this configuration are shown in the top portion of Fig. 74. For both detector pairs one sees a strong peak centered near the 8.5 Mrads^{-1} expected for a 100 G external field.

Immediately after taking this data the external field was turned off while maintaining the temperature at 2 K. The cosine transforms for this zero field arrangement are shown in the bottom portion of Fig. 74. There are two striking features to observe. First, the peak from the F-B data is now completely missing. The disappearance of this peak may be simply understood in

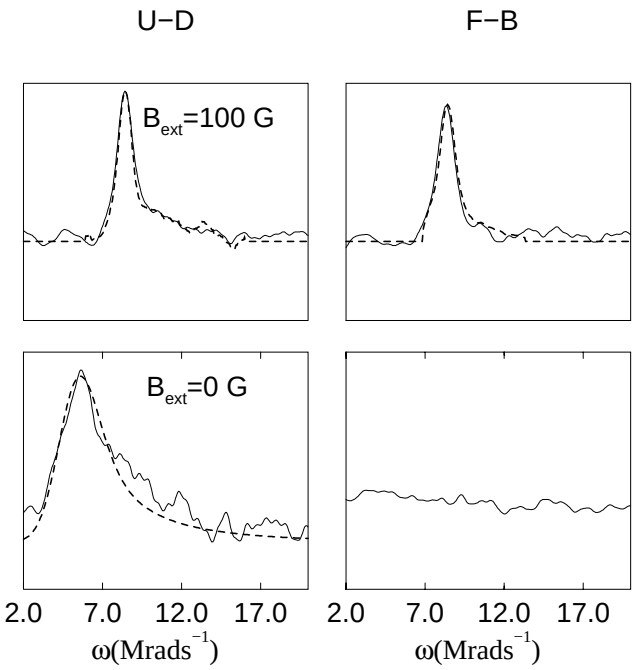

Fig. 74. Fourier transforms for the data from the U-D and F-B detector arrays for BSCCO single crystals. The top set was for field cooled and the field still applied. The bottom pair were taken immediately after $B_{ext.}$ was set to 0. All data were at 2 K. The dashed line in the upper left is our prediction from the data of the lower left, see text. The dashed line of the lower left is derived from a vortex lattice model with λ_{ab} =2000 Åand a local field variation of 13 G.

that the muons are precessing around a field totally aligned along the **c** axis so that the angle the spin makes with respect to this direction is constant. Second, the peak in the U-D data has shifted to about 70 G, as would be expected for precession about only the field component along the **z** direction, i.e., $< b_z > \approx$70 G and b_y=0.

With the external field off, the U-D cosine transform for the BSCCO remained invariant at 2 K and 10 K for time periods of at least an hour. This implies that the field along **c** axis was pinned at these temperatures. If the vortices were truly three dimensional, as in the tilted stack structure in the lower middle of Fig. 73, and if they maintained a 3D integrity through this sample as the field was turned off, vortices at their ends would have to move a distance ≈0.05 mm, half the crystal thickness, in order to form their final vertical stacks. We believe such motion to be inconsistent with the observed pinning. Further, to maintain a constant magnetic flux through the sample, pancake vortices would have had to enter and leave through the sample sides as the field was reduced to zero. This too is inconsistent with the observed pinning. Thus the pancake vortices must not be arranged with tilted correlations which would lead to a trapped tilted average field, but may at most have **c** axis aligned correlations. With only pinned **c** axis correlations, the magnetic field in the **ab** planes is just the applied field component, i.e., even at 2 K the **ab** planes are transparent to magnetic fields. This agrees with the suggestion of Clem, illustrated at the lower right of Fig. 73, that for sufficiently weak interplanar coupling, the vortices would form stacks along the **c** axis.

To test this transparency notion we predicted the Fourier transform of the top left of Fig. 74 from the data of the lower left of Fig. 74 as follows: When an applied field is present, the local magnetic field would arise from a **z** distribution, dn/db_z, as determined from the data of the lower left of Fig. 74, plus a fixed component in the **y** direction. The probability of b is then:

$$\frac{dn}{db} = \frac{dn}{db_z}\frac{db_z}{db}; \;\; b^2 = b_y^2 + b_z^2 \,. \tag{4}$$

Thus from Eq. 3 we expect:

$$\tilde{P}_{yy}(\omega) \propto \frac{dn}{db_z}\frac{b_z}{b} \,. \tag{5}$$

The dashed curve in the top left of Fig. 74 is the result of this transformation of the data of the bottom left of that figure plus a residual background component. Further, we can predict from Eqs. 2 and 3 that

$$\tilde{P}_{yz}(\omega) = \frac{b_y}{b_z}\tilde{P}_{yy}(\omega) \,. \tag{6}$$

The dashed line in upper right of Fig. 74 is this prediction. Thus, we see that an assumption of perfect **ab** transparency, combined with a fixed **c** oriented pancake correlation allows us to predict the applied field case in excellent agreement with experiment.

For comparison, we performed a similar experiment using a large single crystal of YBCO with pinning inclusions. As for BSCCO, the YBCO sample was first field cooled to 2 K in an applied field of about 100 G, 45 degrees from the **c** axis, and at 2 K the applied field was then turned off. The cosine transforms at the lowest temperatures with field off are identical to those with the field on. This implies that the vortices are 3 dimensional and completely pinned.

Vortex motion

The muon's polarization parallel to a static local field at the muon's site remains fixed. But if the local field has fluctuating components perpendicular to its local average these will lead to a slow loss of polarization proportional to $\exp(-(\gamma_\mu b_\perp)^2 \tau t)$.

For most studies of superconductors it would be expected that local vortex density fluctuations give rise to the largest field fluctuations. These field fluctuations, for the case that the field is applied parallel to

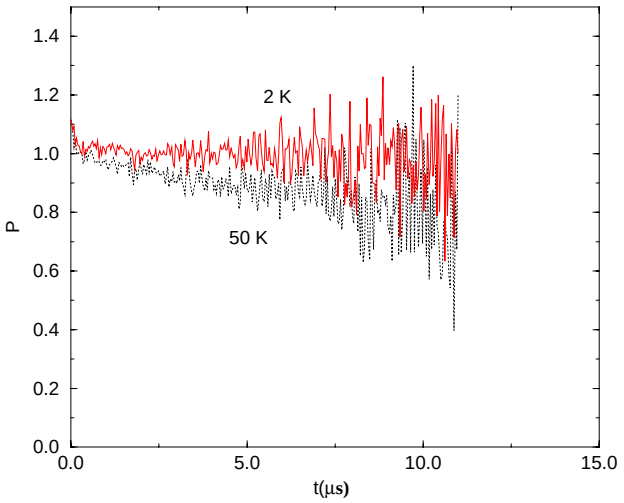

Fig. 75. The longitudinal depolarization in BSCCO for a 100 G field 45 degrees from the **c** axis.

the one of the principal axes, are parallel to the vortices themselves and hence parallel to the average field and therefore produce no perpendicular field and no depolarization. But if the average field is tipped relative to **c**, longitudinal depolarization experiments can be carried out.

For our study of off-axis fields in BSCCO we used a 100 G field at 45 degrees from the **c** axis and an initial polarization roughly along the y axis. After first calibrating the detectors with a field along the x direction we obtained the polarization component parallel to the applied field seen in Fig. 75.

That we can see depolarization at 50 K is evidence for local fluctuations of the magnetic field. Note that in the case of a field 45 degrees from the **c** axis and with currents dominantly in the **ab** planes the field fluctuations will be along the **c** axis and hence have components perpendicular to the average field.

We propose to carry out high statistics measurements of all the samples and for a variety of applied fields to measure the temperature and field dependence of τ.

Experiment 774
Muonium dynamics in GaAs
(B. Hitti, S.R. Kreitzman, TRIUMF)

The goal of this experiment is to further the understanding of hydrogen dynamics in the technologically important compound semiconductor GaAs. Direct resonance techniques are not practical and since the muon is an electronic analogue of the proton in these materials μSR can be used to extract much of the relevant information. Experiment 774 is a long term research project in which we plan to use the various techniques of muon spin rotation/relaxation (μSR) to obtain dynamical information similar to our highly successful results in Si.

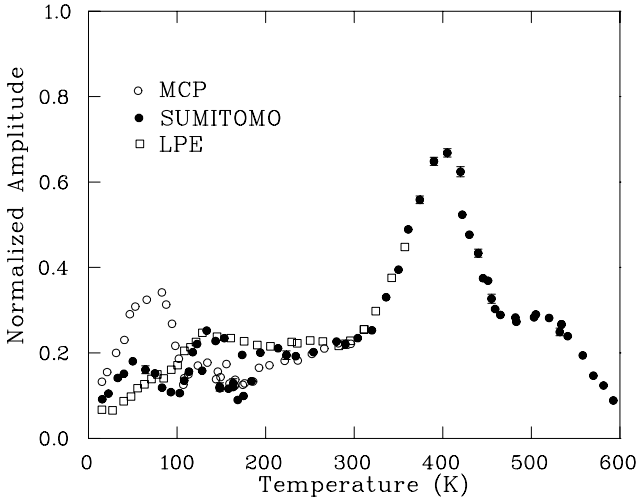

Fig. 76. The temperature dependence of the diamagnetic fraction in two commercial undoped semi-insulating GaAs samples (MCP and SUMITOMO) and in a high quality n-type (2×10^{13} cm^{-3}) liquid phase epitaxy (LPE) GaAs sample.

To date (c.f. Fig. 76) we have used the radio frequency (rf)μSR technique to measure the temperature dependence of the diamagnetic fraction in two commercial semi-insulating (SI) samples and one high quality liquid phase epitaxy (LPE) n-type sample with carrier concentration of about 2×10^{13} cm^{-3}. Several differences are apparent in the behaviour of the diamagnetic amplitude measured in the three samples. Starting at low temperature the peak near 50 K observed in the two commercial samples is not present in the LPE sample. The diamagnetic amplitude in the LPE sample increases monotonically up to 100 K similar to some of the doped Si samples where the increase was shown to result from the ionization of shallow dopant. Between 100 and 300 K, the two commercial samples show a complicated behaviour while the LPE sample is flat at about 20%. In all three GaAs samples the diamagnetic fraction does not increase at the expected ionization temperature of the neutral muonium states, about 100 K for Mu^0_{BC} and 200 K for Mu^0_T. The data below room temperature indicate the presence of intrinsic defects related to deviation from ideal stoichiometry and structure control the material properties of commercial SI samples and make it impossible to obtain sample independent data.

The diamagnetic amplitude measured in the SUMITOMO sample starts to increase above room temperature and peaks near 400 K. This is followed by a plateau centered around 500 K and then a second drop. Only few points are available from the LPE sample above room temperature but the presence of the EL2 defect in commercial material dictates that it is very important to gather high temperature (LPE) data before drawing any conclusions about the nature of the

400 K peak. Finally, the drop centered around 550 K is expected to result from charge exchange involving electrons thermally ionized across the bandgap.

Overall, it is clear that more easily comprehensible results will be obtained from the LPE samples (which have much lower defect concentrations than commercial SI samples) and future experiments will initially concentrate on these. Two μSR techniques are at our disposal. The rf-μSR experiment detects a given centre independently of whether it is formed promptly upon muon implantation or slowly by a transition from a precursor state, and thus detects *final* state amplitudes. In contrast the more standard transverse field (TF) technique is limited by the requirements of phase coherence to detect states that form only rapidly within a small fraction of the (high) frequencies associated with any precursor state. These two techniques are complimentary in the information they provide, viz. the initial and final occupancy fractions of the various charge states in the material. Our plans are therefore to utilize rf-μSR measurements (which are state selective) to complete the temperature dependence of final state diamagnetic amplitude and to obtain analogous data for the two neutral states. TF experiments (which can be obtained simultaneously for all states) will then give us the required temperature dependence amplitudes of the prompt states.

Experiment 776
Rare-earth materials with disordered spin structures
(D.R. Noakes, Virginia State)

This experiment is a muon spin relaxation (μSR) study of RE-Mg-Zn (RE = rare earth) quasicrystals and PrP_x induced moment "spin glasses", motivated by the common features in the results of Expt. 665 (Al-Mn-Si quasicrystals) and Expt. 640 (low carrier density Kondo-lattice CeNiSn and related materials). Results of our study of the rare earth quasicrystals, discussed in the previous Annual Report, have now appeared in Phys. Lett. A [Noakes *et al.*, Phys. Lett. **A238**, 197 (1998)].

The rare earth quasicrystals behaved magnetically like fairly standard dense-moment spin glasses, with some interesting particular details, and a further addition to the mystery of power-exponential relaxation. In contrast, our PrP_x failed to exhibit spin-glass freezing (in spite of freezing reported in the literature), and instead showed unusual paramagnetic dynamics, which require some explanation.

Normally, when magnetic moments in a sample are static, causing a static field distribution at the muon sites, this will generate faster relaxation of polarization than when the moments become dynamic. A fast enough fluctuation rate should even decouple the moments from the muon, leaving no evidence of the moments. This behaviour is seen with the standard Gaussian distribution of local fields and simplistic strong-collision dynamics, which are completely random. This then is the representation of ordinary paramagnetic materials in μSR. Dilute spin glasses are known to have Lorentzian field distributions in their frozen states and also show dynamic decoupling at higher temperatures, in their paramagnetic states. Strong-collision dynamics do not decouple the Lorentzian distribution, however, and in the 1980's Uemura showed that local-environment correlations in dilute spin glasses modify the dynamics so that decoupling still occurs.

It was then a surprise to find that in PrP_x samples, zero-field (ZF) and (LF) μSR spectra below 40 K fit best to strong-collision-dynamic Lorentzian Kubo-Toyabe relaxation functions. At first, the indications of this were weak, because while the generic features of strong-collision-dynamic Lorentzian relaxation have been known for a long time, there are no closed-form expressions for it. To fit, interpolation tables can be developed from numerical simulations, and good approximations must be used when parameters move outside the range of those tables. J.H. Brewer had developed the required tables in the 1980's, but the equally essential approximations had not been identified, because there had been no data that needed them until now. For a Gaussian distribution with width $B_{\rm rms}$ and applied longitudinal field B_{LF} it is known (from NMR) that in the limit of fast fluctuations $\nu \gg \Delta$ (where $\Delta = \gamma_\mu B_{\rm rms}$, the muon Larmor precession frequency in $B_{\rm rms}$) the relaxation becomes exponential with rate:

$$\lambda_G \cong \frac{-2\Delta^2 t/\nu}{1+(\omega_{LF}^2/\nu^2)},$$

where $\omega_{LF} = \gamma_\mu B_{LF}$. We have found that for a Lorentzian distribution of width $B_{\rm hwhm}$ in the same case (applied LF, $\nu \gg a = \gamma_\mu B_{\rm hwhm}$),

$$\lambda_L \cong \frac{-4at/3}{\sqrt{1+(\omega_{LF}^2/\nu^2)}}.$$

Incorporating this into the TRIUMF standard MSR-FIT program, we have obtained reasonable fits to all our PrP_x data.

There then is the question of how strong-collision dynamics can take place in a Lorentzian field distribution in PrP_x, when they do not occur in ordinary dilute spin glasses. Ordinary spin glasses feature stable magnetic moments. When dynamics begin as temperature is raised, individual moments change orientation without changing magnitude. This moment stability is a crucial feature in the local environment model

leading to correlated local field dynamics and fluctuation decoupling in dilute spin glasses. PrP, however, exhibits "singlet ground state" magnetic effects. The praseodymium electronic moment is generated by a $J = 4$ angular momentum state of its unpaired electrons, the individual J_z substates of which have charge-multipole moments which interact with the "crystalline electric field" at each Pr site generated by all the other charges in the lattice. This causes energy differences, between the nine J_z states, that can be from ∼1 K to hundreds of K effective temperature. In PrP, it happens that the Pr ground is an isolated non-magnetic singlet state, with magnetic excitation states above 60 K. When measurement temperature drops below 60 K, then magnetic states become depopulated, and the magnetic response of the material weakens. Thus PrP has *unstable magnetic moments* below 60 K. The removal of a fraction of the phosphorus ions, to make $PrP_{0.9}$, is supposed to rearrange the J_z levels of Pr ions adjacent to vacancies, make their ground states magnetic, and so generate spin-glass freezing, but we do not see that. Instead, our Lorentzian distribution with strong collision dynamics can be explained by slow fluctuations of each Pr ion out of a non-magnetic ground into a magnetic excited state, and back to non-magnetic again. We plan to present the details of this work at the International Conference on μSR to be held in Switzerland in the summer of 1999.

Neither the rare earth quasicrystals nor the PrP_x samples generated the shallow, static relaxation functions we had observed as the common feature of Mn quasicrystals and Ce(Ni,Cu)Sn alloys, so those still stand in some isolation. Noakes, however, has completed Monte Carlo simulations showing that our idea of "range-correlated moment magnitude variation" (RCMMV), mentioned in last year's Annual Report, does indeed generate the shallow, static relaxation functions observed, and that the depth of the minimum is governed by the correlation length over which ion-moment magnitudes remain the same. A manuscript describing the work has been accepted for publication in J. Phys. Cond. Matter.

Experiment 777
Vortex state of *s*-wave superconductors investigated by muon spin rotation

(R.F. Kiefl, TRIUMF-UBC; G.M. Luke, McMaster; R. Kadono, KEK-IMSS)

Motivation

The goal of Expt. 777 is to elucidate the structure and behaviour of magnetic vortices in conventional superconductors using μ^+SR to prove the magnetic field distribution near the vortex cores. Under Expt. 777, we have measured the core radius and magnetic penetration depth in $NbSe_2$ and recently in $LuNi_2B_2C$.

Many recent articles about conventional superconductors followed the 1989 discovery with scanning tunneling microscopy (STM) of bound states in the vortex cores of $NbSe_2$. These bound states were predicted theoretically in the 1960's, and shown in 1974 by Kramer and Pesch to give rise to a sharp shrinking in the vortex core with decreasing temperature. Recent numerical calculations have confirmed their prediction. These predictions, however, are in strong disagreement with the popular Ginzburg-Landau theory, which predicts a constant core radius at low temperature.

$NbSe_2$

We have previously reported measurements of the temperature dependence of the core radius in $NbSe_2$ at low temperature (see 1997 Annual Report, Experiment 777). A further investigation over a larger temperature range confirmed our earlier findings that the core radius does not shrink dramatically with decreasing temperature. This work is currently being written up.

$LuNi_2B_2C$

In November, we made a series of measurements in the borocarbide $LuNi_2B_2C$ (T_c = 16 K). Initial analysis of the temperature dependence of the vortex core radius in $LuNi_2B_2C$ seems to show a sharp shrinking of the core radius as the temperature is lowered to 2 K. Figure 77 shows the Fourier transform of the muon polarization signal in $LuNi_2B_2C$ at 8 K ($T = T_c/2$) and at T = 2.5 K. Initial analysis of the muon polarization in the time domain suggests that the change in the high-field tail is due to a shrinking of the core radius.

Detailed analysis of the data is ongoing. It is not very clear why this Kramer Pesch effect may occur in a borocarbide but not in $NbSe_2$, both of which belong to the class of conventional superconductors. Furthermore, we expect to have characterized the field dependence of the vortex core radius in $LuNi_2B_2C$ upon completion of the analysis.

Doped conventional superconductors

A decision to begin a collaboration with the KEK-IMSS group has now brought all current μ^+SR research at TRIUMF on borocarbides into Expt. 777. This collaboration will also allow Expt. 777 access to more samples. Recent specific heat measurements comparing $YNi_{1-x}Pt_xB_2C$ with pure YNi_2B_2C and $Nb_{1-x}Ta_xSe_2$ with pure $NbSe_2$ [Nohara *et al.*, (submitted to Phys. Rev. Lett.)] lead us to hypothesize that the introduction of dopants in the superconducting borocarbides and $NbSe_2$ may weaken the previously reported strong field dependence in the vortex core radius. We

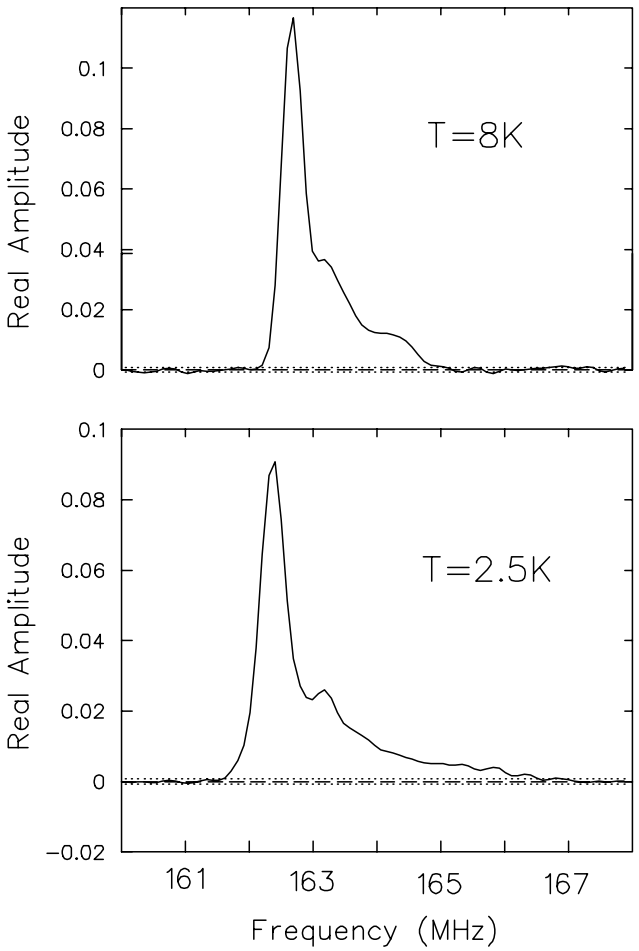

Fig. 77. Fourier transform of the muon polarization signal in $LuNi_2B_2C$ at $T = 8$ K and $T = 2.5$ K, in a field of 12 kG.

hope to characterize the temperature and field dependence of the vortex cores in both $Nb_{1-x}Ta_xSe_2$ and $YNi_{1-x}Pt_xB_2C$ in July, 1999.

MULTI high flux spectrometer

Construction of a new high flux spectrometer, designed to increase the rate of acquisition of muon decay events by a factor of ten, is nearing completion. Currently, the spectrometer is undergoing off-line tests and new software for the data acquistion program is being designed and written. We hope to test MULTI in a high-rate muon beam in May, 1999.

Experiment 782
Non-fermi-liquid behaviour and other novel phenomena in heavy-fermion alloys
(D.E. MacLaughlin, California-Riverside)

Nozières [J. Low Temp. Phys. **71**, 205 (1974)] was the first to suggest that low-lying excitations in Kondo alloys can be described by Landau's fermi-liquid theory, in which there is a one-to-one correspondence between the excitations of the correlated-electron system and those of a free-electron gas. Signatures of this fermi-liquid behaviour are usually taken to be the well-known low temperature thermal and transport properties of a fermi liquid: the susceptibility $\chi(T)$ and Sommerfeld (T-linear) coefficient $\gamma(T) = C(T)/T$ of the specific heat both become constant as $T \to 0$, and the resistivity $\rho(T)$ varies asymptotically as T^2. Fermi-liquid behaviour has also become the canonical description of concentrated Kondo or heavy-fermion systems, principally alloys and intermetallic compounds of lanthanide (Ce,Yb) and actinide (U) ions.

A large and growing number of heavy-fermion alloys are not described by this fermi-liquid picture. Thermal and transport properties of these so-called non-fermi-liquid (NFL) materials as $T \to 0$ seem to fall into a limited number of classes; most (but not all) exhibit a logarithmic divergence of $\gamma(T)$ and a linear departure of $\rho(T)$ from its value at $T = 0$. The susceptibility has been reported to vary either as $1 - b(T/T_K)^{1/2}$ or as $-\ln(bT/T_K)$, where T_K is the Kondo temperature and b is a dimensionless factor of order unity. Nearly all NFL heavy-fermion materials are disordered alloys, and all are found in the neighbourhood of a transition to magnetic order in a temperature-composition phase diagram. Both Ce- and U-based heavy-fermion alloys exhibit NFL behaviour, and it is found both with and without a disordered f sublattice.

A number of mechanisms for NFL behaviour have been proposed, of which two have received the most attention to date. These are (a) the multichannel Kondo effect, first associated with a two-channel quadrupolar Kondo mechanism by Cox [Phys. Rev. Lett. **59**, 1240 (1987)] and since extended to other mechanisms for two-channel Kondo screening, and (b) magnetic instability due to a quantum critical point at zero temperature, the critical behaviour of which generates NFL properties [Millis, Phys. Rev. **B48**, 9887 (1993)]. Our μSR and NMR studies of NFL systems have raised the possibility of a third possible mechanism: an inhomogeneous distribution of Kondo temperatures due to structural disorder in the alloy, referred to as "Kondo disorder".

We have carried out TF-μSR measurements in the nominally ordered NFL compounds UCu_4Pd and $CeNi_2Ge_2$, for the purpose of determining the role of structural disorder in the formation of the NFL state which characterizes these materials. The goals of our μSR studies of NFL behaviour are (a) to ascertain the applicability of disorder-driven mechanisms by measuring the consequent inhomogeneity of the magnetic susceptibility [MacLaughlin *et al.*, J. Phys. Condens. Matter **8**, 9855 (1996)], and (b) to determine whether static magnetism, which could affect bulk properties and masquerade as NFL behaviour, is present.

We have also studied ZF-μSR in the $4f$-electron compound $PrAg_2In$, which exhibits a novel nonmagnetic form of Kondo behaviour at low temperatures. Here it is the nonmagnetic character of the Kondo effect which is the primary subject of interest, although the possibility of NFL behaviour in nonmagnetic Kondo systems has been raised on theoretical grounds.

Non-fermi-liquid heavy-fermion systems

In a recent neutron scattering study on a stoichiometric sample of the NFL heavy-fermion compound UCu_4Pd [Chau *et al.*, Phys. Rev. **B58**, 139 (1998)], it was reported that the data suggest an ordered structure, thus casting doubt on the Kondo disorder mechanism for this compound. The experimental uncertainty in the degree of disorder in these measurements was, however, considerable. Our μSR results show that the μSR linewidth increases strongly with decreasing temperature, in quantitative agreement with our previous results [Bernal *et al.*, Phys. Rev. **B54**, 13000 (1996)] and predictions of disorder-driven theories of NFL behaviour [Miranda *et al.*, Phys. Rev. Lett. **78**, 290 (1997); Castro Neto *et al.*, Phys. Rev. Lett. **81**, 3531 (1998)] in the same sample used for the neutron scattering experiments. Figure 78 shows this agreement in a plot of the quantity $\delta K/(a^*\chi)$ vs. bulk susceptibility χ, where δK is the spread in muon frequency shifts derived from the linewidth and a^* is an effective hyperfine coupling constant. This quantity is an estimator of the relative spread $\delta\chi/\chi$ of the inhomogeneous local susceptibility. The data are compared with $\delta\chi/\chi$ from the Kondo disorder theory in Fig. 78, where it can be seen that the agreement is quite good.

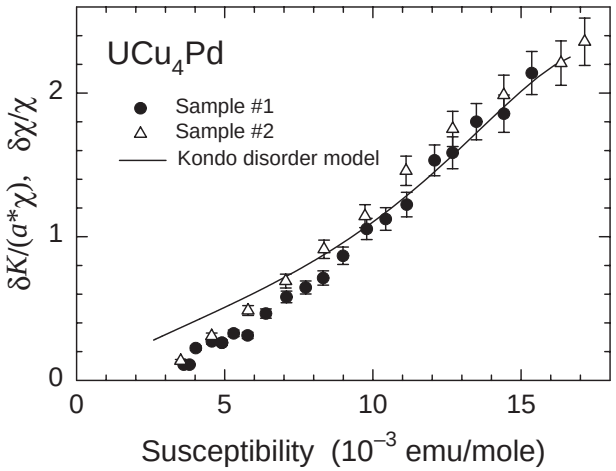

Fig. 78. Dependence of $\delta K/(a^*\chi)$ on bulk susceptibility χ, with temperature an implicit parameter, in UCu_4Pd. Symbols are defined in the text. Sample #1: previously-studied sample [Bernal *et al., op. cit.*]. Sample #2: present sample, used in neutron diffraction studies [Chau *et al., op. cit.*]. Curve: $\delta\chi/\chi$ from the Kondo disorder theory [e.g. MacLaughlin *et al., op. cit.*].

Our results show that the neutron data cannot be taken as evidence for structural order in UCu_4Pd. We argue that the susceptibility inhomogeneity is due to residual disorder, which also dominates the NFL behaviour. The data also show that the correlation length which characterizes the susceptibility inhomogeneity is short ($\sim$1 lattice spacing or less), and that the low temperature U-moment relaxation rate is rapid ($\sim 10^{12}$ s^{-1} or greater). These results constrain cluster-based models of NFL behaviour, such as that of Castro Neto *et al.* [*op. cit.*], as the clusters can be neither too large nor too slowly fluctuating at the temperatures of measurement.

These results motivated a study of structural disorder in UCu_4Pd using the x-ray-absorption-fine-structure (XAFS) technique [Booth *et al.*, Phys. Rev. Lett. **81**, 3960 (1998)], which discovered unambiguous evidence for Cu/Pd site interchange disorder of the right amount to account for the needed T_K distribution width in the Kondo disorder model.

We have also carried out TF-μSR studies of a powder sample of nominally ordered $CeNi_2Ge_2$, in which transport and thermodynamic properties exhibit NFL behaviour at low temperatures. In $CeNi_2Ge_2$ the linewidth, expressed as a rms spread $\delta K(T)$ of Knight shifts, is found to vary proportionally to the average (bulk) susceptibility $\overline{\chi}(T)$ as measured by the average μ^+ Knight shift $\overline{K}(T)$ (with temperature T an implicit parameter). This is in contrast to the prediction of disorder-driven theories of NFL behaviour, for which $\delta K(T)$ varies as $[\overline{\chi}(T)]^2$ or faster. Thus the quantity $\delta K(T)/\overline{K}(T)$, which is an estimator of the fractional susceptibility inhomogeneity $\delta\chi(T)/\overline{\chi}(T)$, is nearly temperature independent, in contrast to our results in UCu_4Pd (Fig. 78). The observed muon line broadening in $CeNi_2Ge_2$ is of the same order as the anisotropy in the magnetic susceptibility, and can therefore be attributed to anisotropy in the Knight shift rather than disorder. But the observed relative broadening $\delta K(T)/\overline{K}(T)$, after correction of $\overline{K}(T)$ for Lorentz and demagnetization fields, is large enough to obscure a significant contribution of disorder to the linewidth. We conclude that the data obtained to date are inconclusive as concerns the question of a disorder-driven mechanism in $CeNi_2Ge_2$.

Nonmagnetic Kondo effect in $PrInAg_2$

In a seminal paper, Yatskar *et al.* [Phys. Rev. Lett. **77**, 3637 (1996)] reported evidence for unconventional heavy-fermion behaviour in the praseodymium-based intermetallic $PrInAg_2$. This compound is one of only a handful of Pr-based materials which exhibit heavy-fermion or Kondo-like properties. Specific heat,

magnetic susceptibility, and neutron scattering experiments indicate a non-Kramers doublet (Γ_3) ground state due to crystalline-electric-field (CEF) splitting of the Pr^{3+} $^1H_4$ term. The Γ_3 state is *nonmagnetic*, i.e., there are no matrix elements of the magnetic moment operator within its doubly degenerate manifold. A nonmagnetic ground state would make the heavy-fermion-like specific heat anomaly found below 1 K and the enormous low temperature Sommerfeld specific heat coefficient $\gamma(T) \approx 6.5\ \mathrm{J\,mole^{-1}\,K^{-2}}$ quite unexpected, and suggests that $PrInAg_2$ may be a system in which an unusual nonmagnetic path to heavy-fermion behaviour is realized. But such a scenario depends crucially on the nonmagnetic nature of the ground state.

We have obtained two results from μSR experiments in $PrInAg_2$ which support the conclusion of Yatskar *et al.* that the Kondo effect in $PrInAg_2$ is nonmagnetic in origin. First, we observe no temperature dependence of the muon relaxation rate at low temperatures, contrary to what would be expected if the specific heat anomaly involved magnetic degrees of freedom. Second, the temperature and field dependence of the muon relaxation indicates that the CEF ground state in $PrInAg_2$ is in fact nonmagnetic, since the low temperature muon relaxation appears to be due only to nuclear magnetism; no electronic magnetic moment is necessary to understand the observed rates. Quantitative agreement indicates strong *hyperfine enhancement* of the ^{141}Pr nuclear magnetic moment. Hyperfine enhancement is an effect of the hyperfine coupling between the nucleus and the Van Vleck susceptibility of f electrons of a non-Kramers f ion in a nonmagnetic ground state, and only occurs when the Pr^{3+} CEF ground state is in fact nonmagnetic.

Figure 79 shows the relaxation function $G(t)$ at 0.7 K in zero field and a longitudinal field of 100 Oe. The relaxation in 100 Oe (triangles) is much faster than expected if the zero-field relaxation (circles) were due to a static distribution of local fields. Dynamic Kubo-Toyabe fits yield a spread in muon local fields and a fluctuation rate which are quantitatively consistent with nuclear magnetism and only nuclear magnetism, provided that hyperfine enhancement of the ^{141}Pr nuclear moment is taken into account. This is strong evidence against a Pr^{3+} electronic magnetic moment, and correspondingly strong evidence for the nonmagnetic doublet (Γ_3) crystal field ground state required for a nonmagnetic route to heavy-electron behaviour. The data also imply the existence of an exchange interaction between neighbouring Pr^{3+} ions of the order of 0.2 K in temperature units, which should be taken into account in a complete theory of a nonmagnetic Kondo effect in $PrInAg_2$.

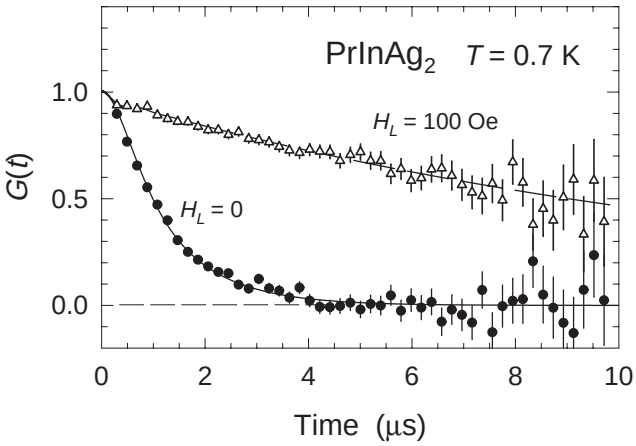

Fig. 79. Dependence of μ^+ relaxation function $G(t)$ on longitudinal applied field H_L in $PrInAg_2$, $T = 0.7$ K. Curves: fits to dynamic K-T model for $H_L = 0$ (solid curve) and $H_L = 100$ Oe (dashed curve).

Experiment 784
The μSR studies of spin-singlet states in oxides
(Y. Fudamoto, G.M. Luke, Y.J. Uemura, Columbia)

Static spin freezing in NaV_2O_5

NaV_2O_5 is the second inorganic compound, after $CuGeO_3$, which has been considered to show a spin-Peierls transition ($T_{SP} = 35$ K). In this report, we present muon-spin relaxation (μSR) studies of pure ($x = 1.00$) and hole-doped ($x = 0.99$ and 0.90) $Na_xV_2O_5$ systems. We have found a static magnetic freezing at $T \sim 11$ K in undoped NaV_2O_5, and suppression of this freezing in Na deficient charge-doped systems. We present a possible interpretation and consider relevance to recent results of thermal conductivity.

The zero-field (ZF) μSR spectra below ~11 K exhibit a fast reduction of muon-spin polarization followed by a slow depolarization of about 1/3 of the total asymmetry, characteristic of relaxation due to coexisting static and dynamic random local fields. The predominant effect of static random fields at low temperatures has been confirmed by decoupling the relaxation by longitudinal fields (LF). Figure 80 shows temperature dependence of (a) the static relaxation rates Δ_i in ZF (b) the dynamic relaxation rates λ_i in ZF and LF=1 kG, and (c) the stretching power β_i above T_f in ZF. Static spin freezing at $T_f \sim 11$ K is indicated by (1) the sudden appearance of static field amplitude Δ below T_f, (2) a maximum of dynamic relaxation rate λ around T_f and (3) a sharp reduction of the stretching power β around T_f. The common slope of λ for $i = 1, 2$ indicates that local fields at the two different muon sites $i = 1, 2$ are subject to the same dynamic process. The high static relaxation rate $\Delta(T \to 0) \sim 35\ \mu s^{-1}$ for the high-field site $i = 1$ cannot be ascribed to a freezing of dilute impurity moments. To account for the

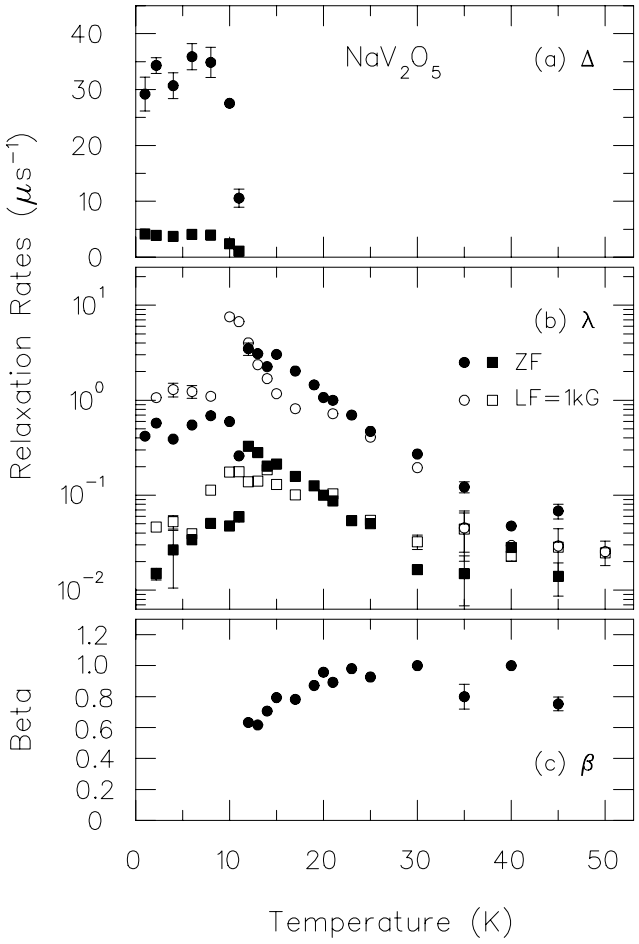

Fig. 80. Temperature dependence of (a) static relaxation rate Δ, (b) dynamic relaxation rate λ and (c) the exponent β, obtained in a (mosaic) single crystal specimen of NaV_2O_5.

observed field amplitude, we have to assume a freezing of at least about 10% of the V^{4+} moments.

We can estimate the fluctuation rate ν of local fields by using a well known relationship $\lambda \sim 1/T_1 = 2\Delta^2/\nu$. Since stretched exponential functions with $\beta \ll 1$ have a very sharp reduction at early times, the relaxation rate resulting from stretched exponential fit with low β values tends to underestimate the average depolarization rate. To compensate for this effect, we calculated $\lambda^* = \ln(2)/[\ln(2)]^{1/\beta} \times \lambda$, and obtained an average fluctuation rate $\nu^* \equiv 2\Delta^2/\lambda^*$. Comparing with the activation behavior $\nu \propto \exp(-E_g/kT)$, we obtain a gap energy $E_g = 77$ K, which is roughly comparable to the spin-gap energy $E_g \sim 110$ K obtained in neutron measurements.

NaV_2O_5 can be doped with holes with a small Na deficiency. The spin-gap formation is suppressed with increasing Na-deficiency, and doped holes are mobile and probably move via variable range hopping. The fast static relaxation observed in pure NaV_2O_5 no longer exists in hole-doped $Na_xV_2O_5$. The dynamic relaxation rate also becomes smaller with increasing hole doping.

In NaV_2O_5, we propose a picture in which a small amount of excess V^{4+} moments, as a subset spin system different from majority V^{4+} moments forming singlet pairs, undergo the spin freezing. The singlet coupling of remaining majority spins may be essential in obtaining effectively high exchange interaction between unpaired V^{4+} spins inferred from a rather high transition temperature T_f. This effective exchange coupling would be suppressed with disappearance of the spin gap, leading to disappearance of the static spin freezing. When the spin gap is suppressed, such subset unpaired spins should be subject to a fluctuation process with all other majority spins. This would reduce the dynamic muon spin relaxation rate via exchange narrowing process, similar to the situation in the paramagnetic state above T_{sp}. The activation behavior of the fluctuation rate ν of unpaired V moments below T_{sp} can be ascribed to thermal excitations of neighbouring singlet pairs to magnetically active triplet states.

Recently, Vasilev *et al.* found a giant peak of thermal conductivity κ of NaV_2O_5 around $T \sim 15$ K. The height of this peak is sharply reduced with increasing hole doping in Na deficient specimens, and the peak disappears when the spin gap is completely suppressed. Phenomenologically, this behaviour seems to be deeply related to our results, and gives another possible support for interpretation of bulk spin freezing (there is no effect of μ^+ in the κ results). The spin freezing below T_f would reduce magnetic scattering of phonons, and thus helps increasing κ. The sharp reduction of κ above T_f can be attributed to increasing spin scattering of phonons.

In summary, we found signatures of spin freezing in undoped NaV_2O_5 around $T_f \sim 11$ K. The spin freezing is suppressed when the spin gap is suppressed in charge-doped Na deficient specimens. Available information favours a picture with spin freezing of more than 10% of magnetic V moments.

This work was supported financially by NSF (DMR-95-10453, 10454, 98-02000; from USA) and NEDO (International Joint Research Grant; from Japan).

Experiment 791
Electronic structure and dynamics of charged muonium centres in semiconductors
(K.H. Chow, Lehigh; R.F. Kiefl, UBC; B. Hitti, TRIUMF)

Results of experiments on muonium in semiconductors are generally considered to be the main source of information on *isolated* hydrogen in semiconductors. Hydrogen is an important impurity which can dramatically affect the electrical and optical properties

of these technologically relevant materials. Recently, we have turned our attention to studying muonium in heavily doped p-type GaAs with the intention of addressing the issue of passivation, i.e. formation of muonium-impurity complexes. Observing and understanding this process as it happens at the microscopic level potentially available with using the μSR technique would provide information unobtainable using other techniques used to investigate hydrogen.

A high concentration of dopants is necessary to improve the chance of passivation. At the same time, the existence of many free holes implies that all the implanted muons retain their initial positive charge. Figure 81 shows the temperature dependence of the decay (assumed to have a Gaussian functional form) of the muon polarization taken under zero-field and transverse-field conditions. The results for two samples, one doped at 2.5×10^{19} cm^{-3} and the other at 5×10^{18} cm^{-3}, are shown. Both transverse-field and zero-field data are available for the 2.5×10^{19} cm^{-3} sample. The former is scaled by a constant factor of 1.7 so that the higher temperature (above 530 K) data for both types of experiments agree.

The results can be interpreted as follows: Initially, as the temperature is raised, there is a decrease in the relaxation because of the increasing muon hop rate. Then, by about 530 K, the muon reaches a trap and is essentially static there. The differences between the two concentrations from 300 K to 530 K suggest that it reaches a trap site sooner in the more heavily doped sample, as would be expected. Above 530 K, breakup of the complex occurs and the muon diffuses freely through the lattice. At the highest temperatures shown (≈850 K), charge state changing reactions occur when a sufficient number of free electrons are thermally generated. In this case, the reaction of relevance is $Mu^+ \leftrightarrow Mu^0$, probably involving alternating electron/hole capture. The differences in the two samples are due to the smaller minority electron concentration in the more heavily doped p-type material.

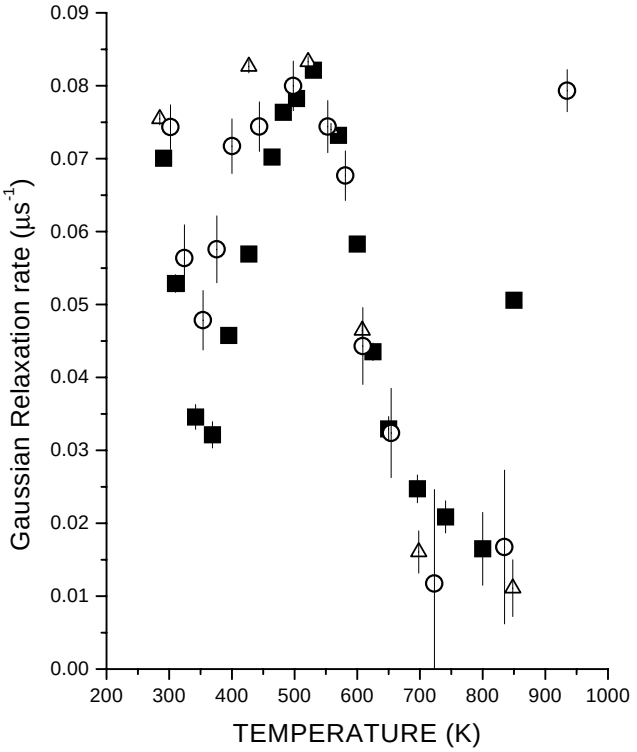

Fig. 81. Gaussian relaxation rate as a function of temperature in p-type GaAs:Zn samples. The open triangles represent the 2.5×10^{19} cm^{-3} and the closed squares indicate the 5×10^{18} cm^{-3} sample studied under zero-field conditions. In addition, the open circles show transverse-field data for the 2.5×10^{19} cm^{-3} sample, scaled as described in the text.

Clearly, more data are needed, such as zero-field measurements in the region below 530 K in the more heavily doped of the two samples. The aim of such experiments is to verify that there is indeed a dependence on the dopant concentration, as would be expected for passivation, and also to extract the relevant rate parameters. Furthermore, experiments below room temperature are also required. Future experiments on this system are likely to be interesting and are eagerly anticipated.

Experiment 792
Muonium in III-V semiconductors

(R.L. Lichti, Texas Tech)

The goals of Expt. 792 were to identify the muonium states in III-V compound semiconductors and to investigate the transitions among those states. Earlier data on GaAs, InP, InAs, and GaSb indicated a trapping peak in the transverse field (TF) μSR diamagnetic signal.

Time allocated to Expt. 792 was used primarily for high field relaxation measurements in these compounds, with some additional high temperature work at low fields. Quadrupolar decoupling curves, i.e. relaxation rate vs. transverse field strength, were obtained at the trapping peaks and at low temperature. These data provided guidance in selecting the field range within which to search for QLCR spectra, which were then pursued in separate experiments. Secondly, longitudinal field depolarization studies were undertaken to investigate transition dynamics, especially for the cyclic charge state transitions present at high temperatures in most semiconductors.

Quadrupolar decoupling curves

Figure 82 shows the quadrupolar decoupling curves for an n-type sample of InP taken at 410 K on the

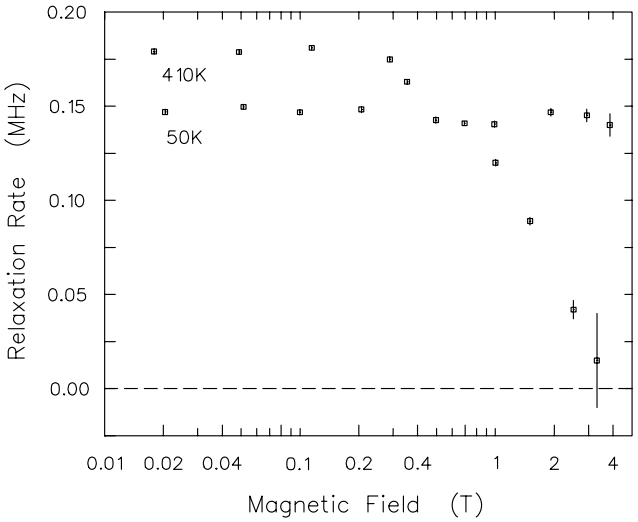

Fig. 82. Field dependence of the TF-μSR relaxation rates at two temperatures for n-type InP. The curve for 410 K implies a site having neighbours with quadrupole moments (In) along $\langle 111 \rangle$ directions.

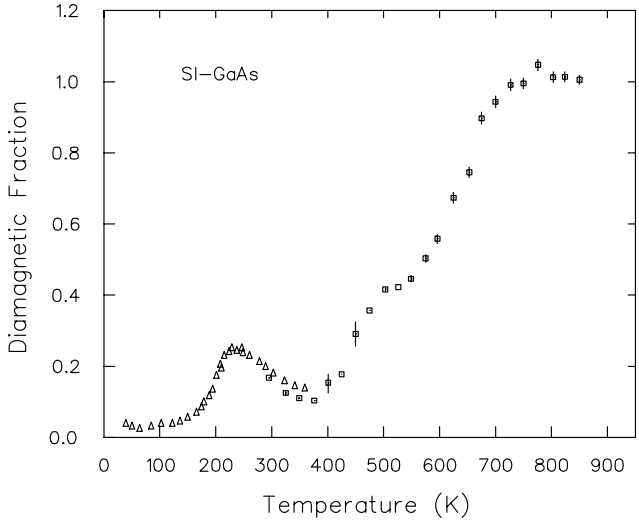

Fig. 83. Temperature dependence of the diamagnetic TF-μSR amplitude in semi-insulating GaAs with at least four transition features. Triangles are data from ISIS to complete the curve.

trapping peak and at 50 K where the low temperature states are still static. These curves imply that these two states have quite different local environments. Zero field relaxation data taken at these temperatures yield quite different local dipolar fields as well. Based on a combination of indirect evidence, we have assigned the state at 410 K to Mu^-. Because the state at 50 K is the same in n- and p-type InP, it has been assigned to Mu^+.

Similar data were obtained for other III-V compounds, and in each case the conclusion is that the higher temperature trapped states are significantly different from the low temperature states. However, precisely identifying either state has proven difficult in most cases.

Transitions in semi-insulating GaAs

Figure 83 displays the diamagnetic TF-μSR amplitude for semi-insulating GaAs indicating several transition regions, subsequently examined in longitudinal fields. The small peak in amplitude below room temperature is Mu^+, identified by the onset of motional narrowing near 200 K as for Mu^+ in p-type GaAs rather than at 550 K which is characteristic of Mu^- [Adams *et al.*, Phil. Mag. **B72**, 183 (1995)]. The rise near 400 K is assigned to Mu^0_T ionization. The additional rise above 550 K represents the effects of a high temperature charge cycle which shows up in these data as a fast relaxing diamagnetic signal. The precise nature of the transitions below room temperature is not completely clear, although they probably represent ionization of Mu^0_{BC} in competition with a BC to T site change for Mu^0, thus may provide additional evidence that the T-site is most stable for Mu^0 in GaAs.

Charge cycle characterization

The main effort in this experiment was to characterize the high temperature cyclic charge state transitions in several III-V compounds. All of the materials investigated except for InP show depolarization from charge cycles. The standard technique applied to this problem is to obtain the temperature and field dependences of relaxation rates in longitudinal field; however, when all the muons are involved in the cyclic transitions TF-μSR relaxation rates probe the same depolarization processes.

Data for GaAs is illustrative: several n-type samples of varying concentration were studied. Above n_e of roughly 10^{17} cm^{-3} the cycles are between Mu^-_T and Mu^0_T as previously characterized in heavily doped samples [Chow *et al.*, Phys. Rev. Lett. **76**, 3790 (1996)]. For semi-insulating and weakly n-type GaAs, the cycles involve Mu^+, with results suggesting a metastable Mu^+_T state rather than the stable Mu^+_{BC}. There is clear evidence for two separate cycles in weakly n-type samples, with only a fraction of the muons involved below 550 K [Lichti *et al.*, Mat. Sci. Forum **258-263**, 849 (1997)]. Figure 84 shows the charge cycle depolarization in two samples, illustrating the difference in onset temperature of $\sim$500 K for the dominant $Mu^0 \rightleftharpoons Mu^+$ cycle compared to $\sim$700 K for $Mu^-_T \rightleftharpoons Mu^0_T$. Although charge cycles have been studied in other III-V materials, such as GaSb, and InAs, the data appear to be much more complicated and the exact nature of the transitions has not been determined.

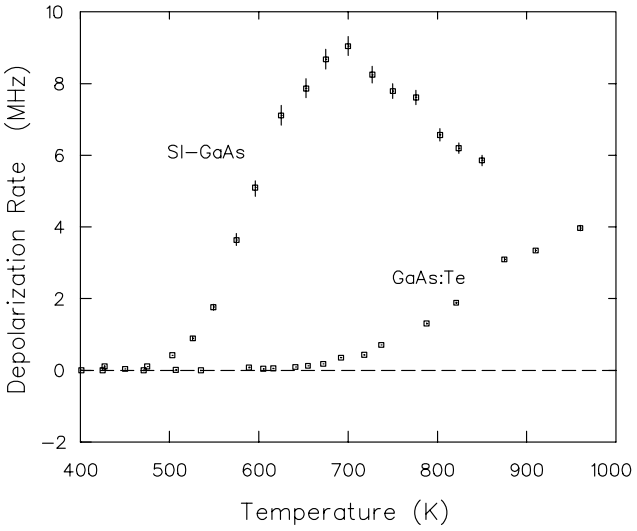

Fig. 84. Mu charge cycle depolarization rates at 10 mT in two GaAs samples: one is semi-insulating where the charged state is Mu^+ and the other is an 8×10^{16} cm^{-3} n-type Te-doped sample where it is Mu^-.

Experiment 804
Muonium in gallium nitride

(R.L. Lichti, Texas Tech)

This experiment continues a long standing effort to understand the behaviour of isolated hydrogen impurities in semiconductors by investigating muonium which provides an analogous and experimentally accessible defect. The group-III nitrides are important widegap opto-electronic materials in which hydrogen plays a significant role, particularly with respect to p-type doping and electrical activity. TRIUMF Expt. 804 and associated experiments at the ISIS Facility represent the first efforts to investigate Mu in GaN.

During the past year we primarily investigated two GaN samples, both very thick (150–200 μm) c-axis oriented films. One is nominally undoped, but has an n-type concentration in the mid–10^{16} cm^{-3} range due to an intrinsic defect. The second is doped with Si to give an n-type concentration of $\sim 10^{18}$ cm^{-3}. Very late in the year we also examined a small GaN single crystal, compensated by Mg doping.

We performed two types of μSR measurements aimed at characterizing the muonium states in GaN and studying transitions among those states. The first technique is a form of muon level-crossing resonance known as QLCR which probes the interaction of diamagnetic muonium centres with neighbouring quadrupolar nuclei. The other series of measurements provide muon spin relaxation functions under three magnetic field conditions, transverse and parallel to the initial polarization and for zero field.

QLCR spectra

Figures 85 and 86 display the QLCR spectra obtained for the more strongly n-type GaN:Si sample at 293 and 150 K, respectively. The room temperature spectrum is identical to that for the undoped film. These figures demonstrate the qualitative differences between spectra obtained above and below ~200 K. The two nearly identical sets of features in Fig. 85 are characteristic of interactions with Ga and are assigned to Mu^- at the two Ga anti-bonding sites (AB_{Ga}) in the GaN wurtzite structure. The single central line associated with each isotope is due to a site with the Mu–Ga bond parallel to the applied field, thus along the c-axis. The weaker doublet for each isotope is assigned to the AB_{Ga} site extending into the channel regions with the bond at roughly 70° to the c-axis. The doublets remain present at lower temperatures while the lines from the c-axis site disappear below 200 K, thereby verifying our initial assignment of the doublet to a separate site

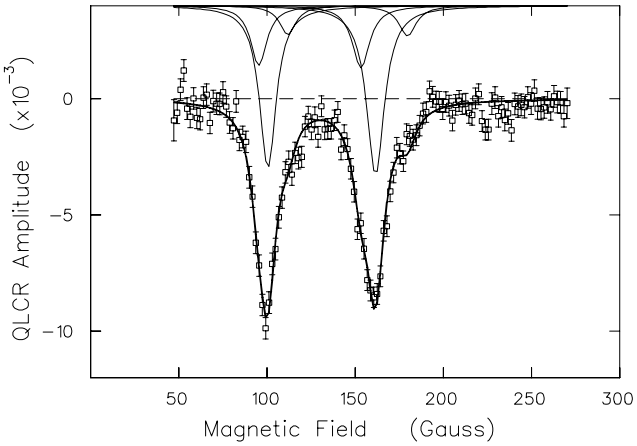

Fig. 85. Room temperature QLCR spectrum for 10^{18} cm^{-3} n-type Si-doped GaN. These features are from interaction with the two Ga isotopes and represent two Mu^- sites.

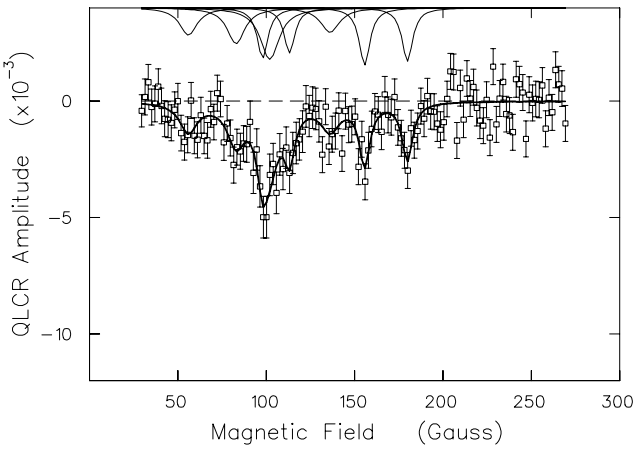

Fig. 86. The 150 K QLCR spectrum characteristic of the low temperature data. Resonance lines not present in Fig. 85 are assigned to nitrogen neighbours of Mu^+ centres.

rather than to more distant neighbours associated with a single on-axis Mu^- centre.

A different set of lines is present in the low temperature spectra as shown in Fig. 86, none of which show the characteristic Ga signature except for the doublets just discussed. The additional features are assigned to interactions of Mu^+ with N nuclei. Mu^+ is strongly attracted to nitrogen, although the specific sites differ for various theoretical approaches. Likely Mu^+ locations include nitrogen anti-bonding (AB_N) and bond-centered (BC) sites: wurtzite has two inequivalent sites of each type. A great deal of additional work remains to complete site assignments and obtain detailed structures.

Low temperature transitions

The temperature dependence of the zero-field (ZF) and weak transverse-field (TF) relaxation functions have been determined for both thick film GaN samples. ZF and TF relaxation rates were also obtained for the compensated GaN crystal in a coarse temperature scan up to 300 K. The two n-type films show similar low temperature relaxation characteristics suggesting a transition near 100 K in the TF data and a jump in the ZF static Kubo-Toyabe width, Δ_{KT}, near 200 K accompanied by growth of the KT amplitude for higher temperatures. The increase in Δ_{KT} occurs in the region where the QLCR spectrum changes; therefore, it can be correlated with occupation of the on-axis AB_{Ga} site for Mu^-. The ZF relaxation also has a weakly relaxing component over the full range and a small exponentially relaxing amplitude above 300 K and at very low temperatures. The weakly relaxing amplitude decreases below the 200 K increase in the KT amplitude and is tentatively assigned to Mu^+ states. A missing fraction in the TF diamagnetic amplitude is consistent with existence of paramagnetic Mu^0 centres. The TF-μSR diamagnetic amplitude dips near 150 K consistent with a transition out of one charged state and at higher temperature into the second one, in general agreement. Preliminary analysis on the compensated crystal also supports these general assignments. This sample does not show the Mu^- zero-field KT signal, consistent with a lack of electrons.

Motion of Mu^-

The Kubo-Toyabe component in the zero-field data is dynamic above roughly 500 K and was fit assuming motion of Mu^-. Figure 87 shows the hop rates for the undoped GaN film. The barrier obtained for the 500 to 850 K activated region is 0.98 ± 0.03 eV. This is very close to the value from ISIS data on the GaN:Si film and for a powdered GaN sample in which only the Kubo-Toyabe component was observed. It is not clear at present which sites are involved in the Mu^- motion.

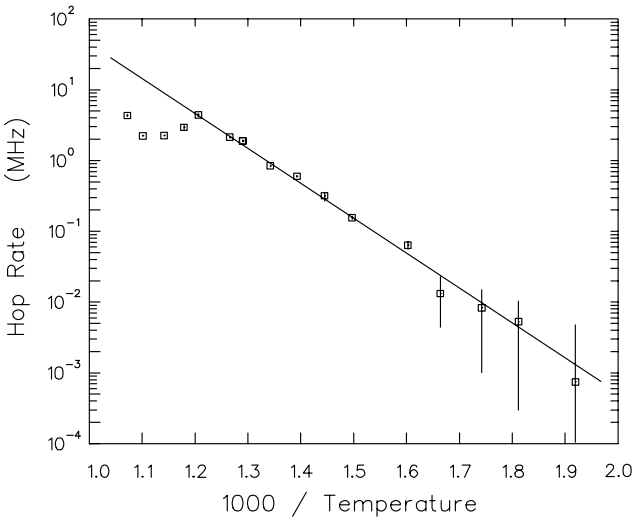

Fig. 87. Hop rates for Mu^- motion extracted from the dynamic Kubo-Toyabe zero-field component in undoped GaN.

High temperature transitions

Data on both the undoped and Si-doped films show a change in behaviour at the very highest temperatures, seen in Fig. 87 as a deviation below the activated curve for temperatures above 850 K. The ZF data for the undoped film also show a small exponential amplitude with an increasing rate in this region, generally consistent with the onset of charge cycles as implied by a TF relaxation feature associated with a small fraction of the muons. Other transitions are also apparent. The KT amplitude increases from about 40% of implanted muons below 700 K to nearly 65% by 900 K and the exponential component representing ~10% of the muons shows a sharp divergence in the rate constant near 600 K. These features suggest a transition from a Mu^0 state into Mu^-.

We examined the undoped film at high temperature in longitudinal fields to identify features associated with transitions, particularly high-T charge-state cycles. Hyperfine decoupling curves at room temperature and at 540 K imply that an isotropic Mu^0 state is present, while the field dependence of one relaxing component suggests possible involvement of an anisotropic Mu^0 state in charge cycles at 850 K. Figure 88 shows the relaxation rates associated with the more strongly relaxing LF component at high temperatures at two fields, 10 and 200 mT. These data are consistent with cyclic charge state transitions in GaN involving a small fraction of Mu states.

We plan to pursue questions left open by these very promising initial results and expect significant progress as thicker films and better quality GaN samples become available in the near future.

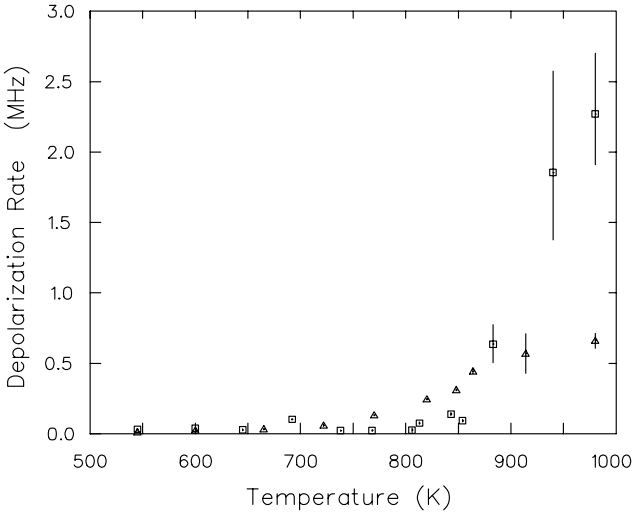

Fig. 88. Temperature dependent longitudinal relaxation rates in undoped GaN at 10 mT (squares) and 200 mT (triangles) implying cyclic Mu charge-state transitions.

Experiment 809
Muonium localization in solid methanes
(V.G. Storchak, Kurchatov Inst.; J.H. Brewer, CIAR/UBC)

Light particles such as electrons, muons, impurity atoms and isotopic defects often propagate by quantum tunneling in solids; a key question in such nonclassical transport is whether the tunneling is coherent or incoherent, i.e. whether a wave-like or particle-like description is appropriate. This in turn depends on the particle's interaction with the environment. One of the possible channels for localization of a particle is through its interaction with lattice excitations (phonons, librons, magnons etc.). At low temperatures, such excitations are frozen out, in which case conventional understanding suggests that the only possible channel for particle localization is the introduction of crystal disorder, which thus may dramatically change the transport properties of a solid. A well-known example is the spatial localization of electron states near the Fermi level in a disordered metallic system, which leads to the "Anderson transition" [Anderson, Phys. Rev. **109**, 1492 (1958)] into a dielectric state: coherent tunneling of a particle is possible only between levels with the same energy (e.g. between equivalent sites in a crystalline lattice); in the case of strong randomness, states with the same energy may be too spatially separated for tunneling to be effective.

We have been exploring the quantum diffusion of the light *neutral* muonium ($Mu = \mu^+ e^-$) atom in *insulating* crystals composed of molecules, in particular CH_4 and CD_4, where *orientational ordering* causes localization of interstitial Mu by creating a source of *weak, short-range* disorder.

The transport properties of a neutral particle in a simple crystalline insulator (e.g. a monatomic or ionic crystal) depend only on the phonon modes of the lattice. For crystals composed of molecules, an additional contribution enters from the rotational degrees of freedom of the molecules. Two extremes are possible: the molecules may rotate almost freely in the crystal or the rotational motion may be severely restricted and hence transformed into torsional excitations (*librons*). Since typical rotational frequencies of molecules in crystals are still much higher than the particle bandwidth, in the first extreme the energy levels for a particle moving in different unit cells are degenerate and therefore particle dynamics remain unperturbed. In the second extreme the anisotropic interaction between molecules (which causes orientational ordering in the first place) changes the crystalline potential so that this degeneracy is lifted. As far as the particle dynamics are concerned, this splitting of the energy levels of adjacent sites acts as an effective disorder. To demonstrate this, we studied muonium dynamics (by measuring the Mu spin relaxation rate in weak transverse field) in solid methanes (CH_4 and CD_4), which undergo orientational ordering at 20.4 K and 22.1 K, respectively. (Partial orientational ordering starts in CD_4 at 27 K.)

The experiments were performed on the M13 beam line at TRIUMF and on the EMu beam line of the ISIS Pulsed Muon Facility at the Rutherford Appleton Laboratory. Atomic muonium was detected by observing the precession signal at the characteristic muonium frequency in a weak transverse magnetic field H. Relaxation of Mu is caused by modulation of its hyperfine interactions with nearby nuclei (parameterized by a NHF coupling constant δ) as the Mu atom diffuses through the crystal. The muonium relaxation rate T_2^{-1} has a simple form in two limits: if muonium "hops" from site to site at a rate $\tau_c^{-1} \gg \delta$ (*fast hopping* limit), then the transverse relaxation rate is given by $T_2^{-1} \approx \delta^2 \tau_c$. For very *slow* diffusion ($\tau_c^{-1} \lesssim \delta$) muonium spin relaxation takes place on a time scale shorter than τ_c and $T_2^{-1} \approx \delta$.

Figure 89 shows the temperature dependences of the muonium T_2^{-1} in solid CH_4 and CD_4, extracted from the spectra by fitting single-exponential relaxation functions. The strong temperature dependence of T_2^{-1} abruptly levels off between about 45 K and 55 K in CH_4 and between about 32 K and 40 K in CD_4. Such behaviour in the fast hopping regime indicates that the Mu hop rate stays constant in the indicated temperature ranges in both crystals. At the lowest measured temperatures (below about 20 K), T_2^{-1} again levels off in both crystals due to Mu localization, giving $\delta_1 \approx 5 \times 10^7$ s^{-1} for CH_4 and $\delta_2 \approx 8 \times 10^6$ s^{-1} for CD_4. The ratio δ_1/δ_2 is about twice as large as the

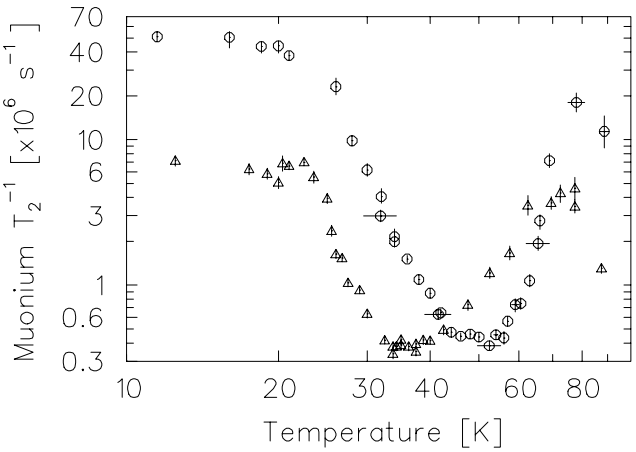

Fig. 89. Temperature dependence of muonium relaxation rate T_2^{-1} in solid methanes (circles: CH_4; triangles: CD_4) in a weak transverse field $H = 5$ G.

ratio of proton to deuteron magnetic moments, which is not really surprising – the NHF interaction, which governs muonium relaxation in all the substances where Mu atoms have been observed, need not scale with the magnetic moments of neighbour nuclei with different spins. Other candidates for the muonium spin relaxation mechanism, such as spin-exchange reactions with possible paramagnetic impurities (e.g. O_2) or electrons from the muon track, were ruled out by measurements in longitudinal magnetic and electric fields.

Figure 90 shows the temperature dependences of the muonium hop rate τ_c^{-1} in the solid methanes, extracted in the regime of dynamical averaging using the values of δ obtained above. At high temperatures – above 55 K for CH_4 and above 40 K for CD_4 – the hop rate in both crystals *increases* with *decreasing* temperature. This is an unambiguous manifestation of quantum diffusion which has also been recognized for muonium in KCl [Kiefl *et al.*, Phys. Rev. Lett. **62**, 792 (1989)] and solid nitrogen [Storchak *et al.*, Phys. Rev. Lett. **72**, 3056 (1994)]. In the appropriate temperature ranges in both KCl and nitrogen, the muonium hop rate exhibits an empirical temperature dependence $\tau_c^{-1} \propto T^{-\alpha}$ with $\alpha \approx 3$ in KCl and $\alpha \approx 7$ in nitrogen. In solid CD_4 similar fits yield α between 5 and 6 while in CH_4 α is between 7 and 11 depending on the temperature range.

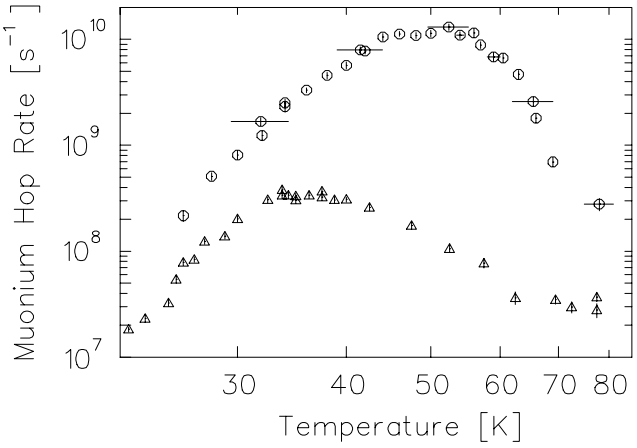

Fig. 90. Temperature dependence of muonium hop rate in solid methanes (circles: CH_4; triangles: CD_4).

The plateaus in $\tau_c^{-1}(T)$ around 45–55 K in CH_4 and 32–40 K in CD_4 must represent the onset of muonium band motion [Kagan and Prokof'ev, *Quantum tunneling diffusion in solids*, in Quantum Tunneling in Condensed Media, eds. Leggett and Kagan (North-Holland, 1992), p.37; Storchak and Prokof'ev, Rev. Mod. Phys. **70**, 929 (1998)], which occurs if the coherence is preserved and the disorder is weak. In this case the hop rate is independent of temperature and we may estimate the muonium bandwidth to be about 3×10^{-2} K in CH_4 and about 10^{-3} K in CD_4. These values may be compared with muonium bandwidths in KCl and solid nitrogen (0.16 K and 10^{-2} K, respectively) [Storchak and Prokof'ev, *op. cit.*].

The band motion does not extend to the lowest temperatures, however: the hop rate begins to decrease with decreasing temperature below about 45 K in CH_4 and about 30 K in CD_4. These data indicate that interstitial muonium atoms undergo gradual localization in methanes at low temperatures where the temperature dependence of the muonium hop rate obeys the power law $\tau_c^{-1} \sim T^{\alpha}$ with $\alpha = 6.8(4)$ in both crystals. In this temperature range the observed power law is believed to be due to two-phonon dissipation in the regime of static destruction of the band [Kagan and Maksimov, Sov. Phys. JETP **57**, 459 (1983)].

This phenomenon can be explained in terms of the slowing down of molecular rotations in the crystal. At high temperatures, when the characteristic time of molecular reorientation $\tau_r \ll \tau_c$, the anisotropic molecular interactions are averaged out and muonium undergoes unperturbed bandlike propagation.

In conclusion, we have presented an observation of the destruction of bandlike motion of light interstitial particles in molecular crystals at low temperatures. We suggest that the particle localization is due to slowing down of molecular rotations and subsequent orientational ordering in these crystals. This study complements our knowledge of the nature of neutral particle localization due to *long-range* disorder.

Experiment 814
μSR studies of unconventional superconductivity in Sr_2RuO_4
(G.M. Luke, McMaster)

Sr_2RuO_4, which is isostructural to the high-T_c cuprate $La_{1.85}Sr_{0.15}CuO_4$, is to date the only known layered perovskite superconductor which does not contain copper. Although first synthesized in the 1950's, its superconductivity was only found in 1994; T_cs of early samples were roughly 0.7 K but have increased to $T_c = 1.5$ K in recent high quality single crystals.

Despite its low transition temperature, Sr_2RuO_4 is of great interest as there is growing evidence for an unconventional superconducting state. In this system, strong correlation effects enhance the effective mass seen in quantum oscillation and Pauli spin susceptibility measurements, in the same way as in ^{3}He. Combining this feature with Sr_2RuO_4's expected tendency to display ferromagnetic spin fluctuations, it was argued that the pairing in Sr_2RuO_4 could be of odd parity (spin triplet) type.

One aspect of the pairing symmetry, the breaking of time reversal symmetry (TRS) can be probed directly. If the superconducting state has a degenerate representation (as is possible for some triplet superconducting states) then TRS can be broken, whereas it cannot be broken for non-degenerate representations (the case for all singlet states). For states with broken TRS, originating from either spin or orbital moments, a spontaneous internal magnetic field can appear below T_c. One can expect a finite hyperfine field at a magnetic probe for the case of spin moments, while (for both the spin and orbital cases) spontaneous supercurrents in the vicinity of inhomogeneities in the order parameter would create a magnetic field near impurities, surfaces, and/or domain walls between the two degenerate superconducting phases.

Two single crystals of Sr_2RuO_4 were grown at Kyoto University using a floating-zone method with an infrared image furnace. The superconducting T_cs were 1.478 K and 1.453 K with widths of 48 mK and 40 mK respectively, where T_c is defined as the sharp rise in the dissipative component of the ac-susceptibility and the width is its full width at half maximum. Sample A was cleaved and arranged in a mosaic so that the c-axis was normal to the sample's planar surface and parallel to the initial muon polarization while sample B was cut using a diamond saw such that the c-axis lay in the plane of the sample.

In Fig. 91 we show ZF-μSR asymmetry spectra measured at T = 2.1 K and T = 0.02 K for sample B where $\mathcal{P}_\mu \perp c$. Spectra for sample A ($\mathcal{P}_\mu \parallel c$) are qualitatively similar. From Fig. 91 we see that the relaxation rate is quite small both above and

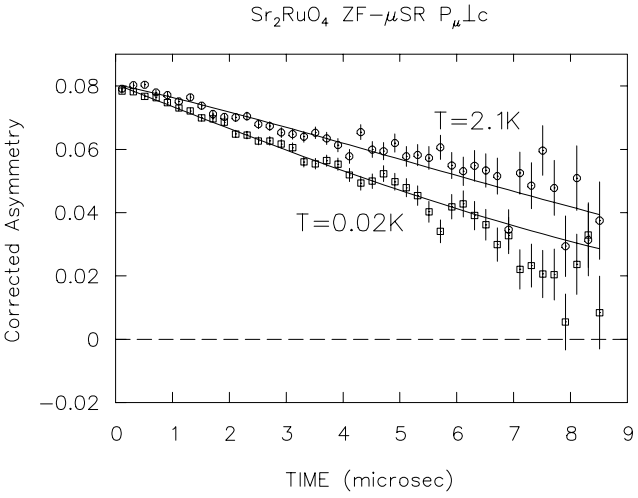

Fig. 91. Zero field μSR spectra measured with $\mathcal{P}_\mu \perp c$ in Sr_2RuO_4 at T = 2.1 K (circles) and T = 0.02 K (squares).

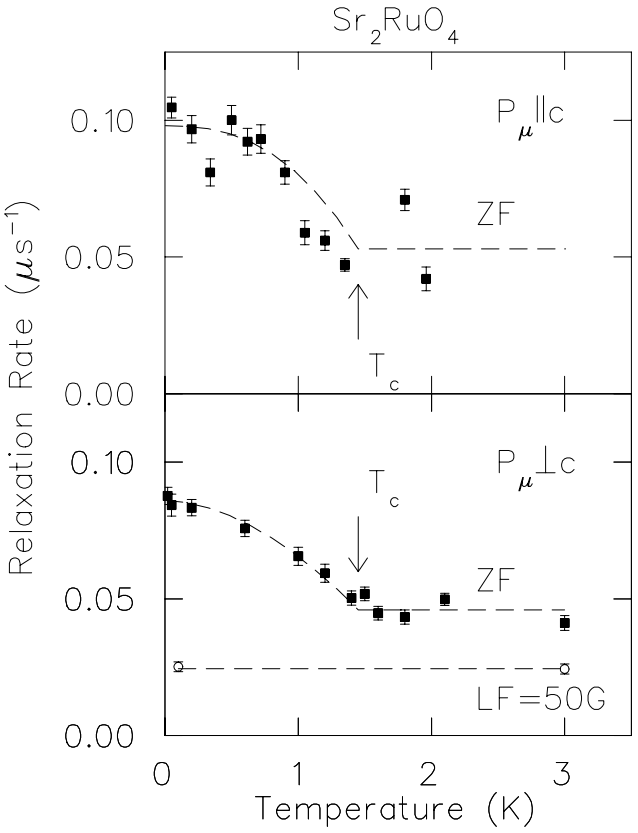

Fig. 92. Zero field relaxation rate Λ for the initial muon spin polarization $\parallel c$ (top) and $\perp c$ (bottom). T_c from ac-susceptibility indicated by arrows. Circles in bottom figure give relaxation rate in $B_{LF} = 50$ G $\perp c$. Curves are guides to the eye.

below $T_c = 1.45$ K, but that there is greater relaxation at lower temperature. This increased zero field relaxation could be caused by either (quasi-)static or fluctuating magnetic fields. We see in the lower panel of Fig. 92 that the relaxation in $B_{LF} = 50$ G is the same above and below T_c, which indicates that the zero field

relaxation must therefore be due to spontaneous fields which are static on the μs timescale.

We tried several functional forms for the additional relaxation below T_c; fits to precessing (cosine) or Gaussian forms were essentially equivalent to each other, but were significantly worse than an exponential in fitting the data. Fitting the spectra to the product of a Kubo-Toyabe (using common values of $\Delta = 0.02,\ 0.06\ \mu s^{-1}$ for samples A and B respectively, for all temperatures to account for the nuclear dipole fields) and an exponential $\exp(-\Lambda t)$ to characterize the additional relaxation due to the spontaneous magnetic field, we plot Λ vs. T in Fig. 92 for samples A ($\mathcal{P}_\mu \parallel$c) and B ($\mathcal{P}_\mu \perp$c). Also shown are the superconducting T_cs as determined by ac-susceptibility. We see a clear increase in Λ with an onset temperature around $T_c = 1.45$ K for both orientations indicating the presence of a spontaneous magnetic field appearing within the superconducting state. In principle, this spontaneous field could originate either from a TRS breaking superconducting state or with a purely magnetic state which coincidentally onsets near T_c. Very recently, we performed additional measurements on a third sample with a reduced $T_c = 0.9$ K and found that the spontaneous field onset at that reduced T_c. Thus, we conclude that since this field is so intimately connected with superconductivity, its existence provides direct evidence for a time reversal symmetry breaking superconducting state in Sr_2RuO_4.

The increased relaxation in the superconducting state is exponential in character. If there were a unique field at the muon site we would observe a precession signal, while a dense collection of randomly oriented field sources results in a Kubo-Toyabe relaxation function. Both the precession and Kubo-Toyabe signals start with a Gaussian form and in the limit of weak characteristic fields are essentially indistinguishable. The exponential form which we observe in Sr_2RuO_4 indicates a broad distribution of fields arising from a dilute distribution of sources. This is consistent with the source of the internal field being supercurrents associated with variations in the superconducting order parameter around dilute impurities and domain walls. We see enhanced relaxation in both samples A and B. From this we can conclude that the local field cannot lie purely along the c-axis (this would give no relaxation from sample A). However, any orientation of the local field which has a significant component in the basal plane is consistent with our data.

The increase in the exponential relaxation below T_c is about 0.04 μs^{-1} which corresponds to a characteristic field strength $\Lambda/\gamma_\mu = 0.5$ G. This is about the same as we observed in the B phase of UPt_3 and is in line with theoretical predictions for that material. No theoretical estimates of the characteristic field strength in Sr_2RuO_4 are yet available; however, we would expect them to be comparable to those in UPt_3 as the fields should arise from a similar mechanism.

Several authors have considered the allowed symmetries of pairing states for the specific case of tetragonal symmetry appropriate for Sr_2RuO_4. Spin-singlet pairing leads exclusively to non-degenerate states and the breakdown of TRS would, in general, require additional phase transitions admixing other pairing channels within the superconducting phase, for which there is no experimental indication so far. On the other hand, one can show that in the spin-triplet pairing channel, TRS breaking states appear naturally at the onset of superconductivity, consistent with our experiment. Based on these symmetry arguments we conclude that the present experiment provides strong evidence for Cooper pairing with spin-triplet (p-wave) symmetry: a superconducting analog of the A or A_1 phases of superfluid ^{3}He. The distinction between unitary and non-unitary states in Sr_2RuO_4, however, cannot be done with the present results and has to wait for further studies by other means.

Experiment 831
Magnetic properties of $REBa_2Cu_3O_x$
(M. Pinkpank, D. Andreica, F.N. Gygax, A. Schenck, ETH Zurich; B. Hitti, TRIUMF; J.H. Brewer, UBC/TRIUMF; A. Amato, PSI)

This experiment studies the dynamic behaviour of the magnetic rare earth (RE) moments in $REBa_2Cu_3O_x$. If the Y in the $YBa_2Cu_3O_x$ system is replaced by lanthanide ions (with the exception of Ce, Pr, Tb and Pm), antiferromagnetic ordering of the lanthanide $4f$-moments is observed at low temperatures, without any obvious adverse effect on the superconducting state. The 3D antiferromagnetic ordering in, for example, $HoBa_2Cu_3O_7$, $GdBa_2Cu_3O_x$ and $ErBa_2Cu_3O_x$ occurs, although the lanthanide ions are sandwiched by the superconducting CuO_2-planes. Apparently the superconducting electrons are very narrowly confined to the CuO_2-planes, as also evidenced by the extremely short coherence length along the crystallographic c-axis ($\xi_c \approx 3$Å), and do not overlap with the local $4f$-electrons. The absence of the conduction electrons at the rare earth sites is also implied by Mössbauer data. In view of these features, it is not very clear by what mechanism the observed magnetic order is driven.

In order to gain more insight into the coupling mechanism between the $4f$-moments (dipolar coupling, superexchange, or others), we study the dynamic magnetic properties of $REBa_2Cu_3O_x$ (RE = Ho, Gd, Er) for samples with different oxygen content.

Earlier longitudinal field (LF) μSR measurements

on $HoBa_2Cu_3O_x$ and $GdBa_2Cu_3O_x$ at PSI show a pronounced difference in the temperature and field dependence of the LF relaxation rate.

In $HoBa_2Cu_3O_x$ the Ho^{3+} ions have a total angular momentum $J = 8$. The 17-fold degeneracy of the $^5I_8$ ground state multiplet is completely lifted by the crystal electric field (CEF) in the orthorhombic phase ($x \geq 6.4$). In the tetragonal phase ($x \leq 6.4$) some singlets will combine to doublets. Since the CEF ground state is a singlet, the magnetic moment has to be induced by hyperfine interaction with the nuclear moment or an overcritical exchange interaction, before any magnetic ordering can take place. The LF relaxation rate shows a strong temperature dependence with a maximum at about 5 K. The field dependence of the LF relaxation rate in the superconducting samples at 6 K can be described by a power law. Within the allocated beam time at TRIUMF we were able to show that this is no more the case for non-superconducting $HoBa_2Cu_3O_{6.2}$.

The $^8S_{7/2}$ multiplet of the Gd^{3+} ion in $GdBa_2Cu_3O_{6+x}$ is a pure spin state, and the Gd sublattice orders antiferromagnetically below 2.2 K. The dynamic relaxation rate, as function of the temperature, measured in longitudinal field (LF) μSR, is temperature independent above 20 K, and no field dependence is observed.

In order to get more insight in the different magnetic behaviour of $GdBa_2Cu_3O_x$ and $HoBa_2Cu_3O_x$, we performed LF measurements on $ErBa_2Cu_3O_7$ at TRIUMF. In this system the CEF ground state is a Kramers doublet, and the total angular momentum of the Er^{3+} ion $J = \frac{15}{2}$ is bigger than the angular moment of Gd^{3+}, while the measured relaxation rate λ is smaller. The relaxation rate was found to be temperature independent up to ≈200 K, where muon diffusion sets in. As in $GdBa_2Cu_3O_x$ no field dependence of the relaxation rate was found. The analysis of the data is still in progress.

Experiment 832
Study of the non-magnetic-magnetic transition in the $Yb(Cu_{1-x}Ni_x)_2Si_2$ system

(D. Andreica, ETH Zurich)

Transverse field measurements on $Yb(Cu_{1-x}Ni_x)_2Si_2$

Introduction

We have performed μSR transverse field (TF) measurements on $Yb(Cu_{1-x}Ni_x)_2Si_2$ samples. The aim of this investigation is to obtain information about the Kondo coupling constant J.

The chemical pressure in the $Yb(Cu_{1-x}Ni_x)_2Si_2$ series, obtained by replacing Cu by Ni, drives the system from a non-magnetic ground state in $YbCu_2Si_2$ to a magnetic ground state in $YbNi_2Si_2$. The main interactions which influence the transition are the screening of the Yb's magnetic moment because of the intrasite Kondo effect ($k_BT_K \propto \exp(-1/JN(E_F))$) and the intersite RKKY magnetic interaction ($k_BT_{RKKY} \propto (J^2N(E_F))$). Both interactions depend on the same parameter J, the Kondo coupling constant between the localized and the conduction electrons. Under applied pressure, J is supposed to increase for Ce compounds and to decrease for Yb compounds [Doniach, Physica **B1**, 213 (1977)].

Theoretical background

For rare-earth compounds the corrected μ^+-Knight shift can be written as $K = K_0 + K_f$, where K_0 and K_f correspond to the contributions of the internal fields arising from the polarization of conduction electrons and localized f-moments induced by the external field H_{ext}. At low temperatures, K_f is much larger than K_0 and contains two contributions due to the localized f-moments: the dipole-dipole interaction between the f-moments and the μ^+, and the indirect RKKY interaction producing an additional spin polarization of the conduction electrons at the μ^+ site resulting in an increased hyperfine contact field.

For a polycrystalline sample,

$$Kiso = \frac{A_c}{3}(\chi_\parallel + 2\chi_\perp) + \frac{A_{dip}^{zz}}{3}(\chi_\parallel - \chi_\perp)\,.$$

If the dipolar coupling and the anisotropy of the magnetic susceptibility are known, the value of A_c could be obtained. Since the hyperfine contact coupling constant A_c is proportional with $g = JN(E_F)$, the key parameter for the RKKY and Kondo interactions, its dependence on the Ni concentration x in the $Yb(Cu_{1-x}Ni_x)_2Si_2$ compounds will allow us to monitor the competition between these two interactions close to the non-magnetic-magnetic transition.

Results

TF temperature scans were performed at 6000 G on the $x = 0$, 0.125 and 1 samples. The samples were mounted on an iron oxide disk in order to get rid of any off-sample background signal. The μSR signal for all investigated samples contains 2 components, one of these belonging to a few percent of an impurity phase. For all investigated compounds, the low temperature Knight shift deviates from the linear scaling with the magnetic susceptibility. Some work is still to be done to compute all the contributions to the Knight shift and then the hyperfine coupling constant A_c. The preliminary fit results are plotted in Fig. 93. Only the contributions arising from the samples are displayed.

A similar work performed at PSI by Wiesinger and co-workers [Physica **B230**, 243 (1997)] on the

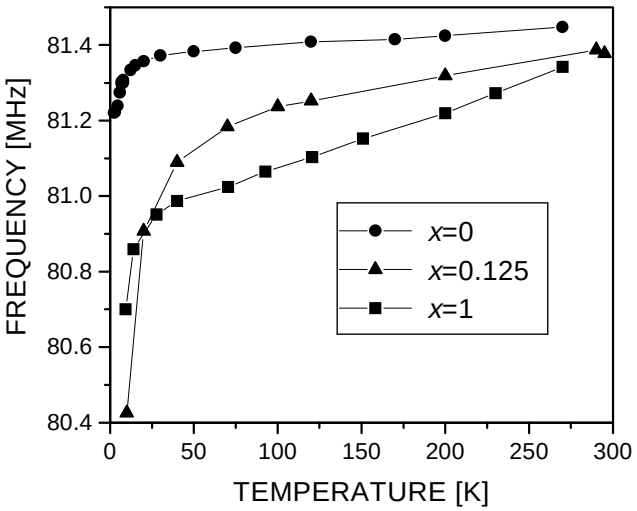

Fig. 93. Temperature dependence of the sample's signal frequency. The transverse field measurements were performed in a field of 6 kG.

effects of Cu substitutions by Al in $CeCu_5$ allows one to compute the A_c dependence on the Al concentration

In the Doniach model, the increase of A_c as a function of Al concentration supports the picture that for high Al concentration the Kondo interaction is dominant. We expect that for $Yb(Cu_{1-x}Ni_x)_2Si_2$ the mirror behaviour will be obtained; that means a decrease of the A_c value with increasing pressure.